3. Electromagnetic methods

3.1 Introduction

- The electromagnetic techniques have the broadest range of different instrumental systems.
- They can be classified as either time domain (TEM) of frequency domain (FEM) systems.

  FEM: use one or more frequencies

  TEM: Measurements as a function of time

Active and passive methods

- EM methods can be either passive, utilizing natural ground signals (e.g. magnetotellurics) or active, where an artificial transmitter is used either in the near field (as in ground conductivity meters) or in the far field (using remote high powered military and civil radio transmitters as in the case of VLF and RMT methods).
- The aim of the measurements is the same as in DC-geoelectrics.

Determination of resistivity

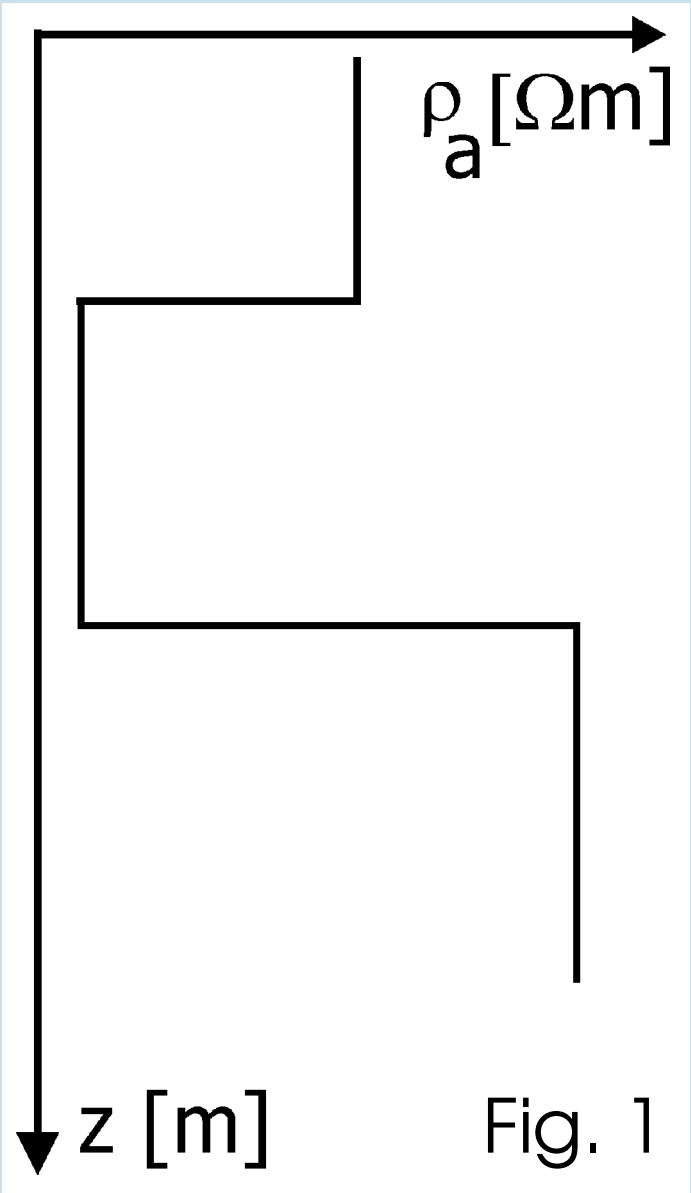

Fig. 1

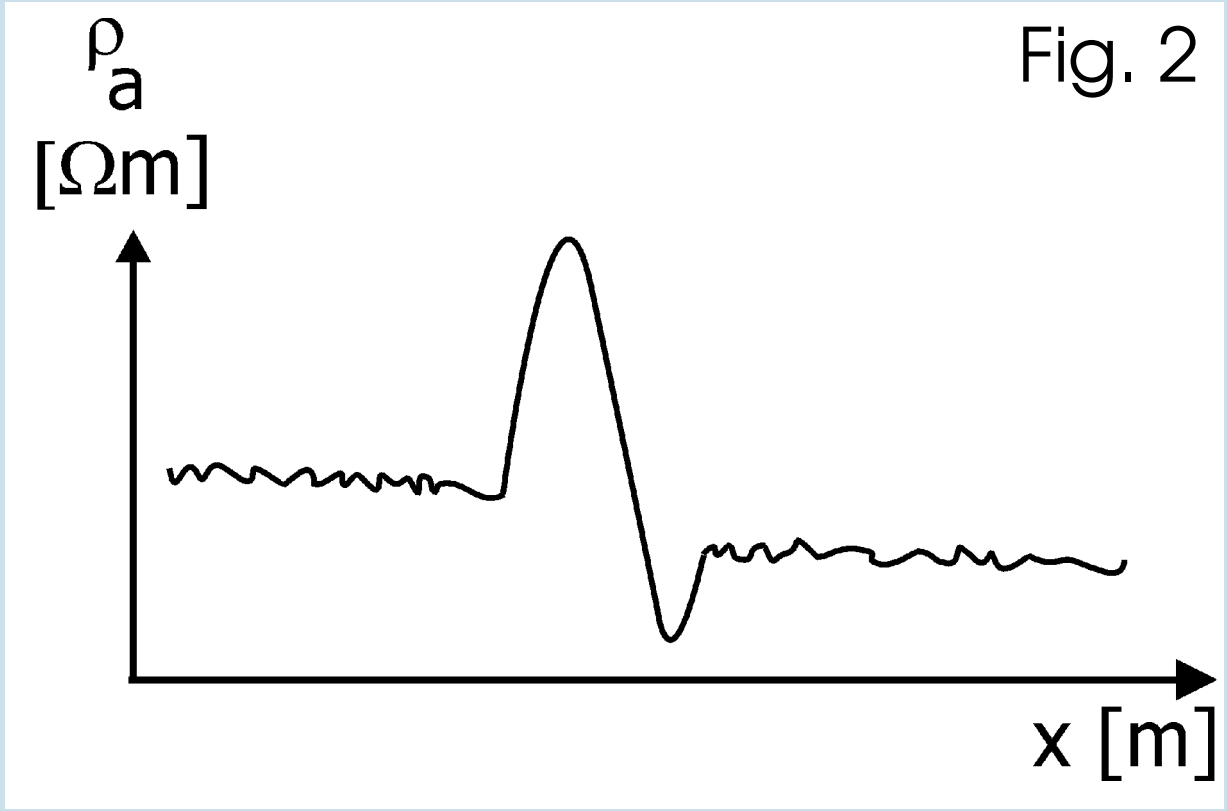

Fig. 2

Determination of resistivity as a function of depth or a function of profile distance.

Advantage of EM-methods

- The main advantage of the EM-methods is that they do not require direct contact with the ground as in the case of DC-electrical methods. Therefore the EM-measurements can be carried out in a faster way than the DC-measurements.
- The range of EM applications is large. It is dependent upon the type of equipment but can be categorized as listed in the table.

Table: The range of applications for EM-surveying (independent of instrument type) [1]

Mineral exploration
Mineral resource evaluation
Groundwater surveys
Mapping contaminant plumes
Geothermal resource investigations
Contaminated land mapping
Landfill surveys
Detection of geological and artificial cavities
Location of geological faults, etc.
Geological mapping
Permafrost mapping, etc.

3.2 Principles of EM surveying

- Electromagnetic (EM) methods make use of the response of the ground to the propagation of the electromagnetic fields which are composed of alternating electric intensity and magnetic force.
- An electromagnetic field may be defined in terms of four vector functions E, D, H and B, where:

E is the electrical field in V/m.

D is the dielectric displacement in Coulomb/m².

H is the magnetic field intensity in A/m.

B is the magnetic induction in Tesla.

Maxwell's equations: Faraday's law

Experimental evidence shows that all electro-magnetic phenomena obey the following four Maxwell equations.

$$\mathrm{rot}\,\mathbf{E} = -\partial \mathbf{B} / \partial t \qquad (3.1)$$

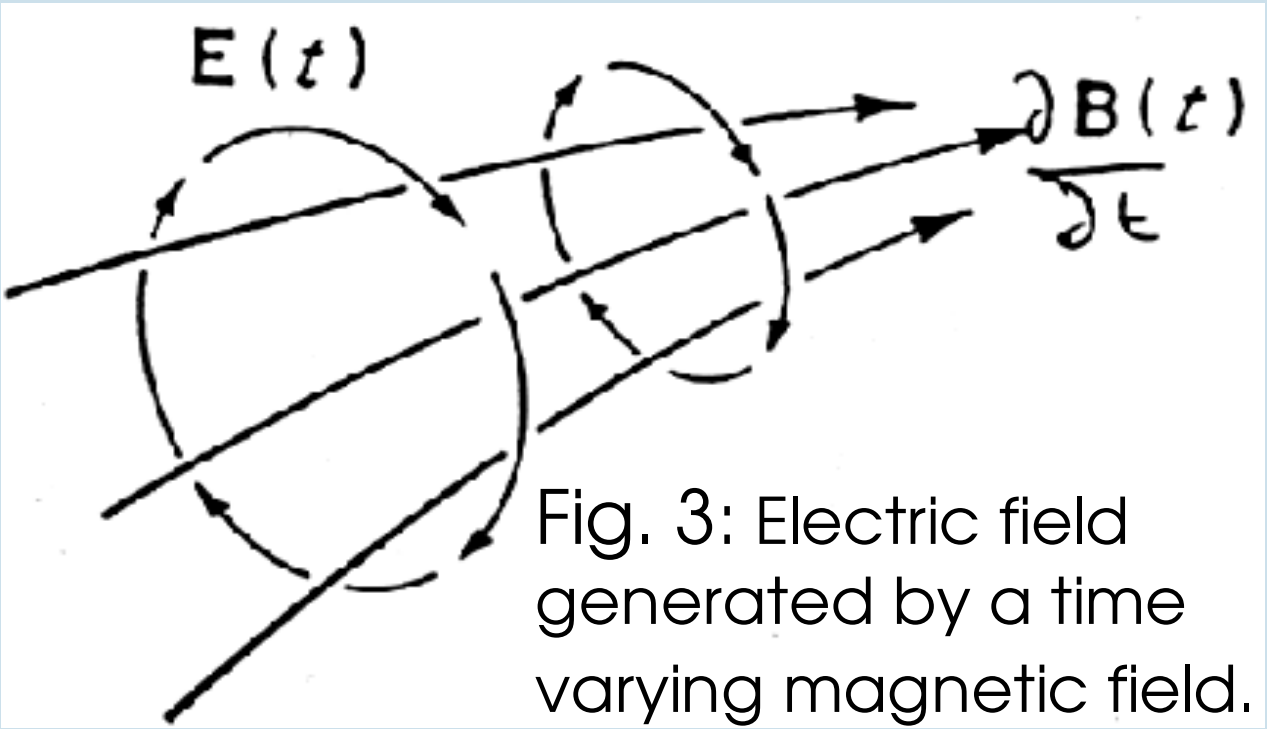

Fig. 3: Electric field generated by a time varying magnetic field.

Faraday's law. It shows us how a time varying magnetic field produces an electrical voltage.

Maxwell's equations: Ampere's law

$$\mathrm{rot}\,\mathbf{H} = \mathbf{J} + \partial \mathbf{D} / \partial t \qquad (3.2)$$

Ampere's law. It shows us how an electric current and/or a time varying electric field generates a magnetic field.

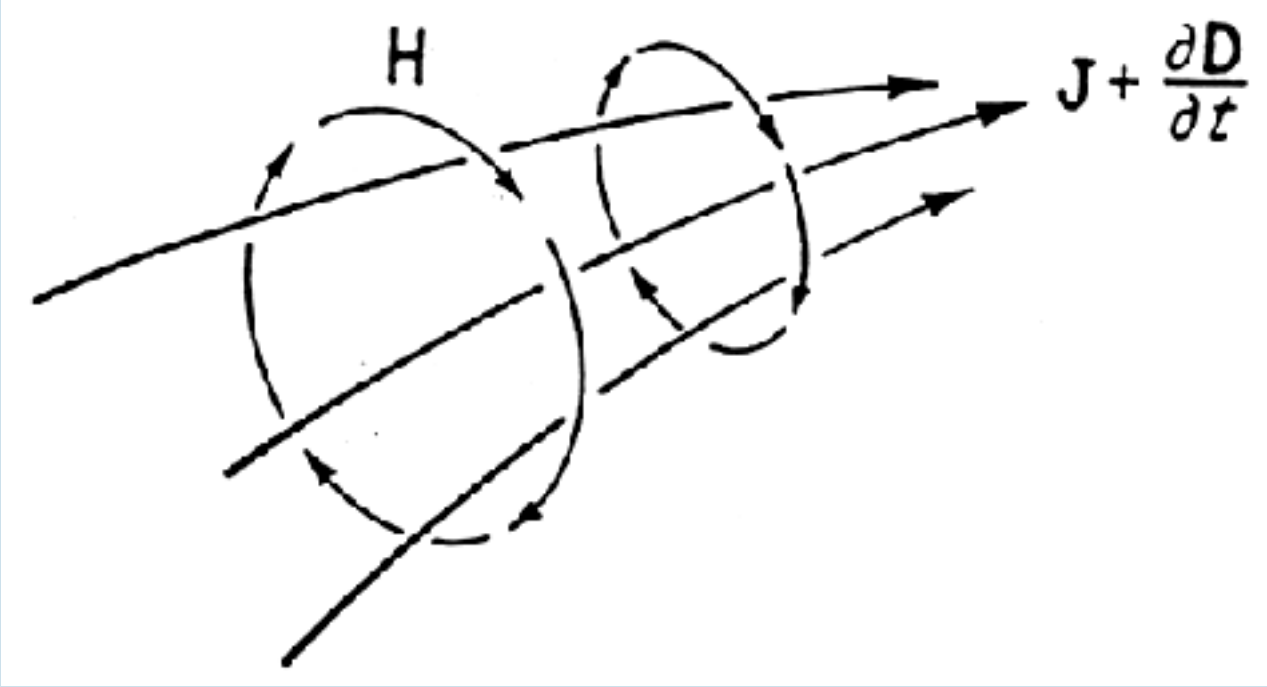

Fig. 4: Magnetic field generated by a time varying electric field.

Maxwell's Equations

$$\mathrm{div}\,\mathrm{B} = 0 \qquad (3.3)$$

It infers that lines of magnetic induction are continuous and there are no single magnetic poles.

$$\mathrm{div}\,\mathrm{D} = \mathrm{q} \qquad (3.4)$$

It infers that electrical fields can begin and end on electrical charges.

Subsidiary equations and wave equation

By using the following subsidiary equations,

$$\mathrm{D}=\epsilon\,\mathrm{E} \qquad \mathrm{B}=\mu\,\mathrm{H} \qquad \mathrm{J}=\sigma\,\mathrm{E}$$

where J = electrical current density in A/m²
q = electric charge in Coulomb/m³
ϵ = electrical permittivitiy
μ = magnetic permeability
σ = electrical conductivity

and the four Maxwell equations the electro-magnetic wave equation can be derived. Such waves, with low attenuation and their relationship are shown in the following figure.

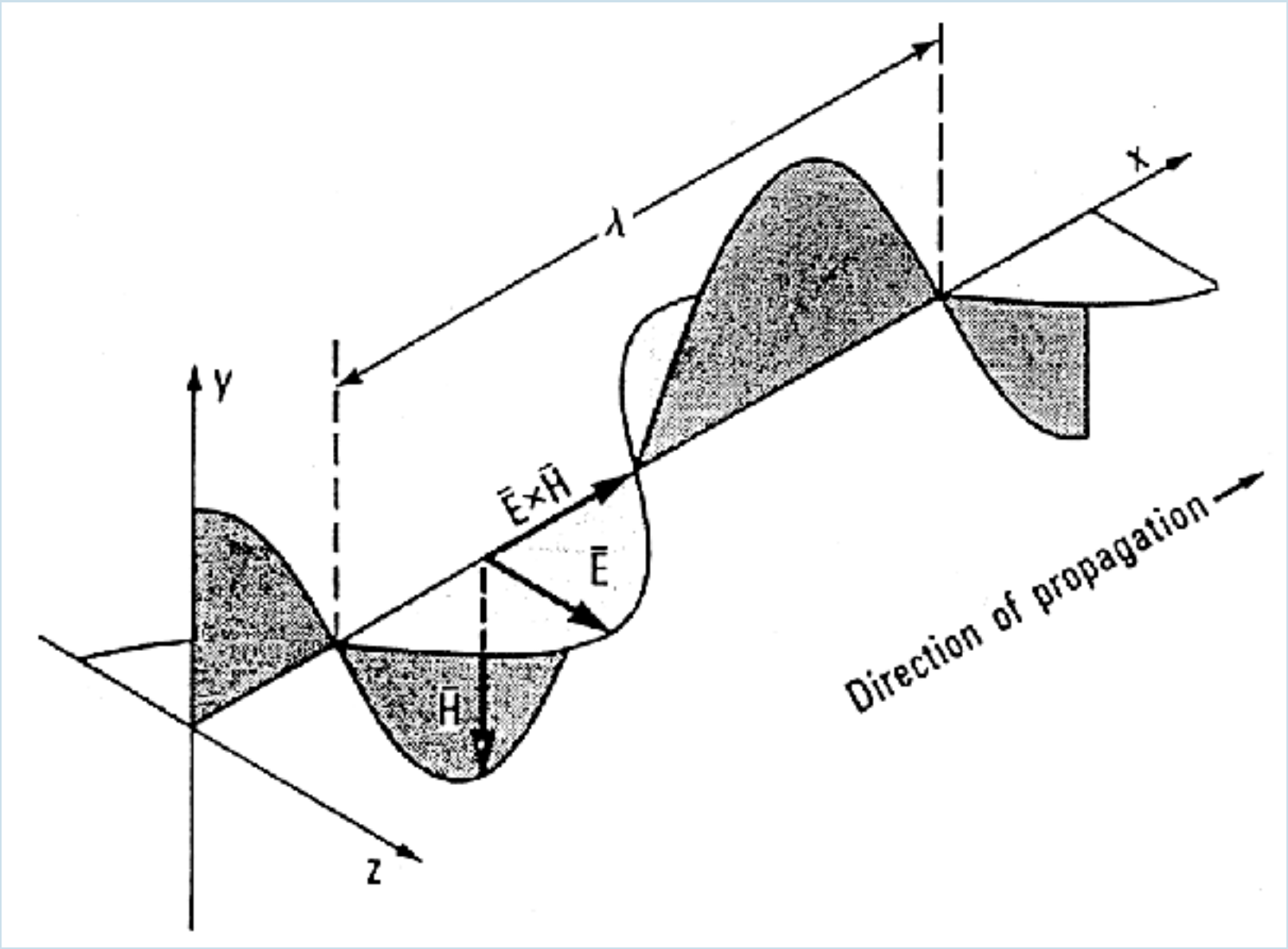

Fig. 5: The electric and magnetic vectors in an electromagnetic wave are perpendicular to each other and to the direction of propagation x.

EM waves and Geophysics

An electromagnetic field can be generated by passing an alternating current through a small core made up of many turns of wire or through a large loop of wire.

For geophysical applications, frequencies of the primary alternating field are usually less than a few thousand Hertz.

The wavelength of the primary wave is of the order of 10-100 km, while the source receiver separation is much smaller.

→ The propagation of the primary wave and associated wave attenuation can be disregarded.

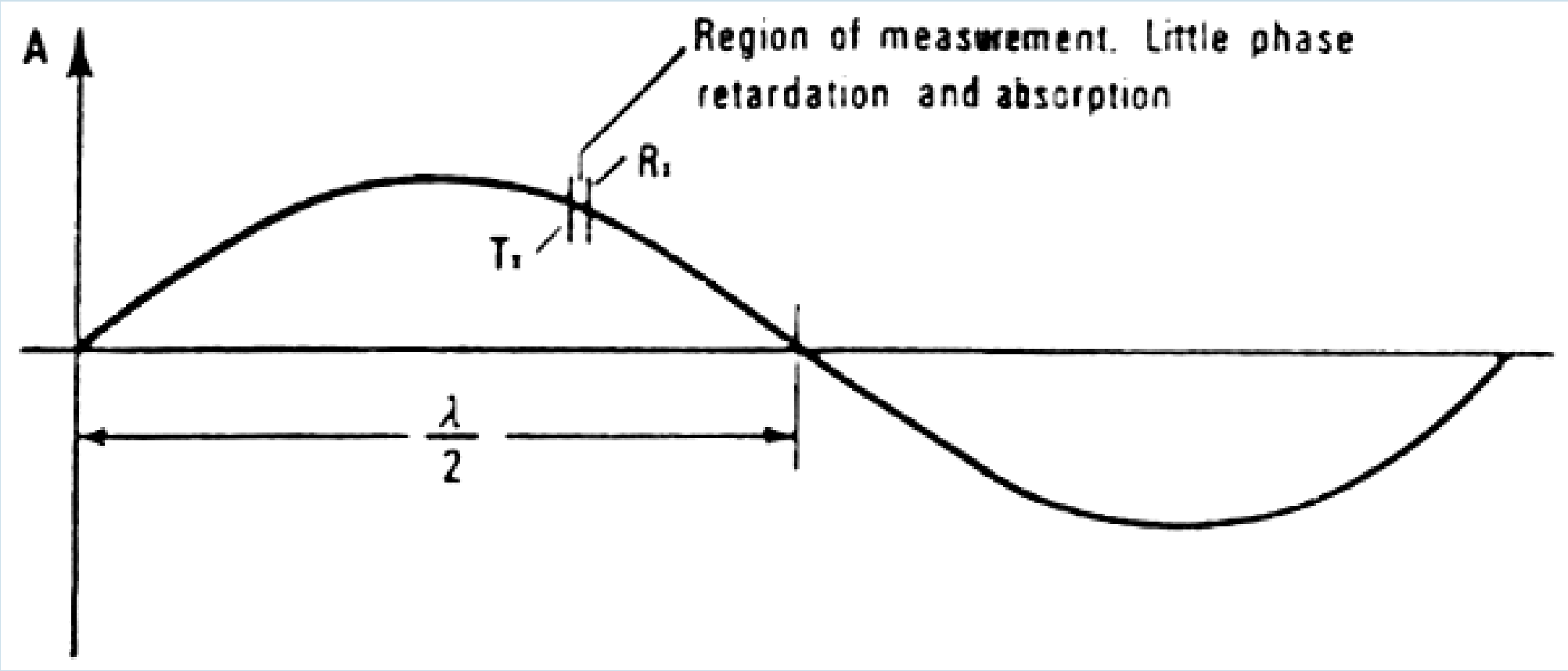

Fig. 6: The physical separation of a transmitter (Tx) and a receiver is very small in relation to the wavelength of the EM waves with frequencies greater than 3 kHz. Consequently, attenuation due to wave propagation can be ignored. [1]

A transmitter coil can be used to generate the primary electromagnetic field which propagates above and below the ground.

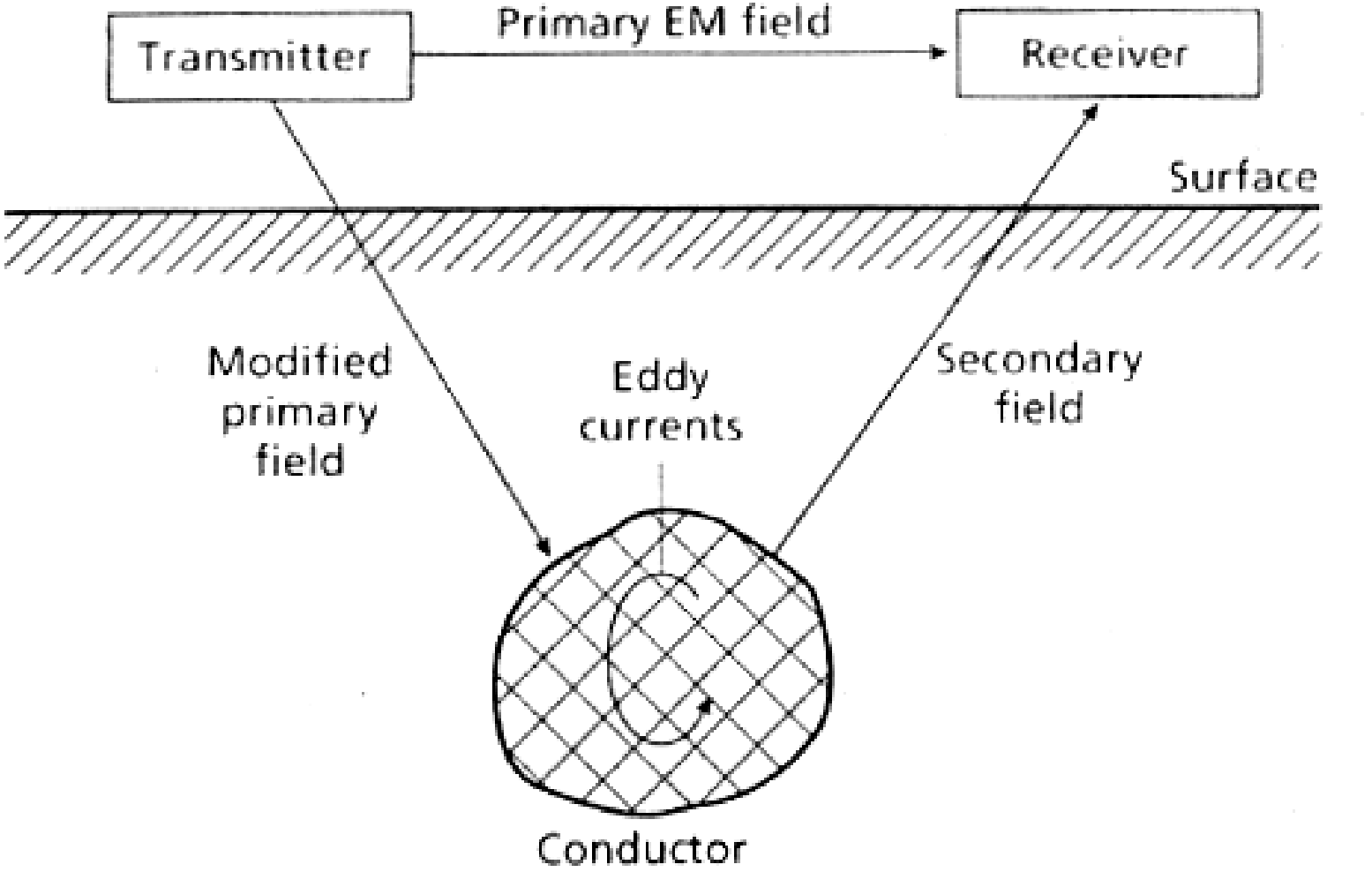

Fig. 7: General principle of electro-magnetic surveying. [2]

Primary and secondary fields

Where the subsurface is homogeneous there is **no** difference between the fields propagated above the surface and through the ground (only slight reduction in amplitude).

If a conductive anomaly is present, the magnetic component of the incident EM wave induces alternating currents (Eddy currents) within the conductor.

The eddy currents generate their own secondary EM-field which travels to the receiver.

Primary and secondary fields

The receiver also detects the primary field which travels through the air.

The receiver responds then to the resultant of the arriving primary and secondary fields.

Consequently, the measured response will differ in both phase and amplitude relative to the unmodulated primary field.

These differences between the transmitted and received electromagnetic fields reveal the presence of the conductor and provide information on its geometry and electrical properties.

3.3 Depth of penetration of electromagnetic fields

- The depth of penetration of an electromagnetic field depends upon its **FREQUENCY** and the **ELECTRICAL CONDUCTIVITY** of the medium.
  The amplitude of EM fields decreases exponentially with depth. The amplitude of EM-radiation as a function of depth relative to its original amplitude A_0 is given by

$$A_d = A_0 e^{-1}.$$

- The depth of penetration can be defined as the depth at which the amplitude A_d is decreased by the factor e^{-1} compared with its surface amplitude. Penetration depth d is given by

$$d[m] = 503\sqrt{\rho[\Omega\,m]/f[Hz]}.$$

Example: Depth of penetration

$$\rho = 10\,\Omega\,\mathrm{m} \quad f = 10\,\mathrm{Hz} \rightarrow d = 503\,\mathrm{m}$$
$$f = 100\,\mathrm{Hz} \rightarrow d = 159\,\mathrm{m}$$
$$f = 1000\,\mathrm{Hz} \rightarrow d = 50.3\,\mathrm{m}$$

3.4 Principle of Slingram method

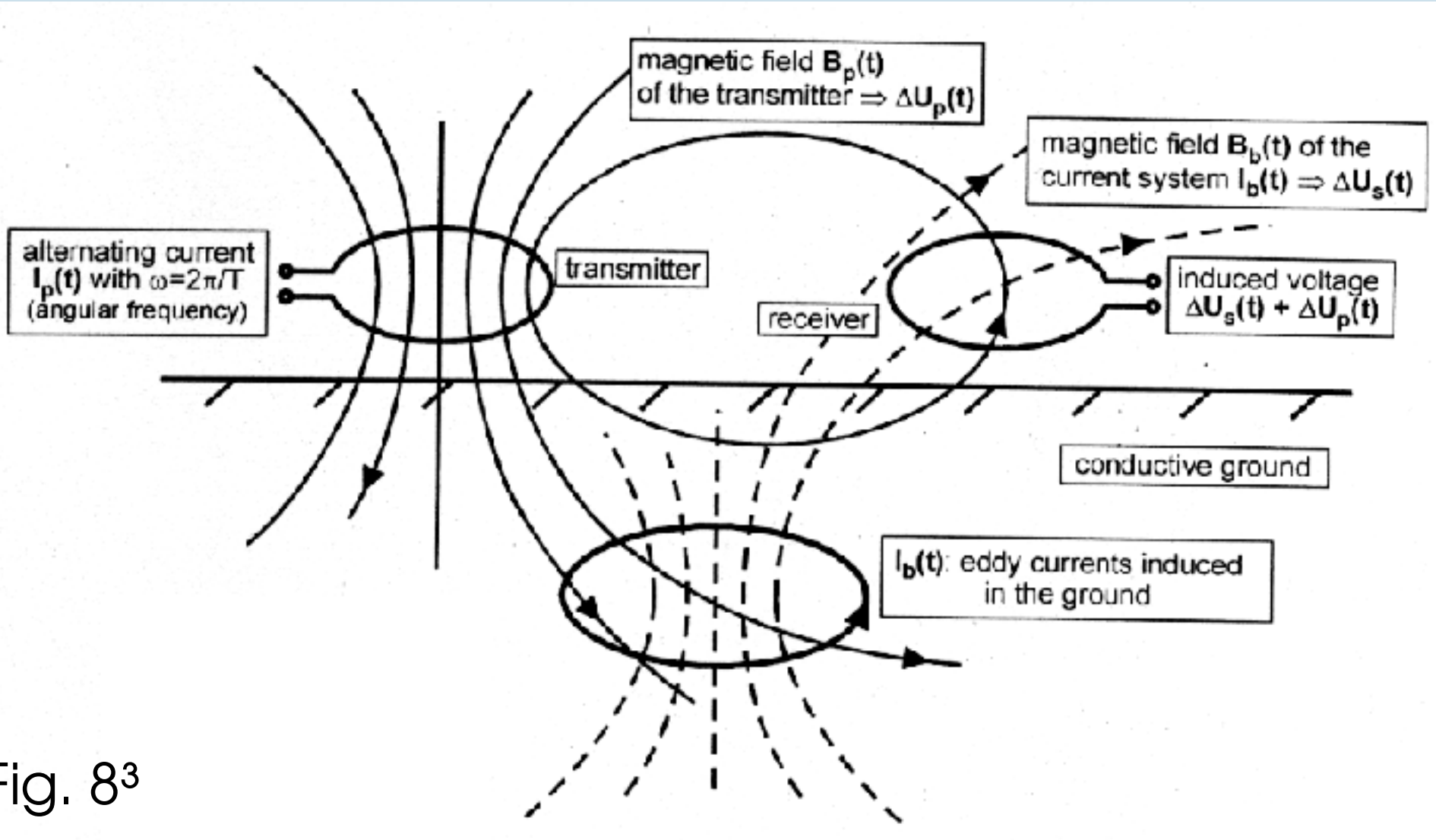

Fig. 8[3]

Principle of Slingram method

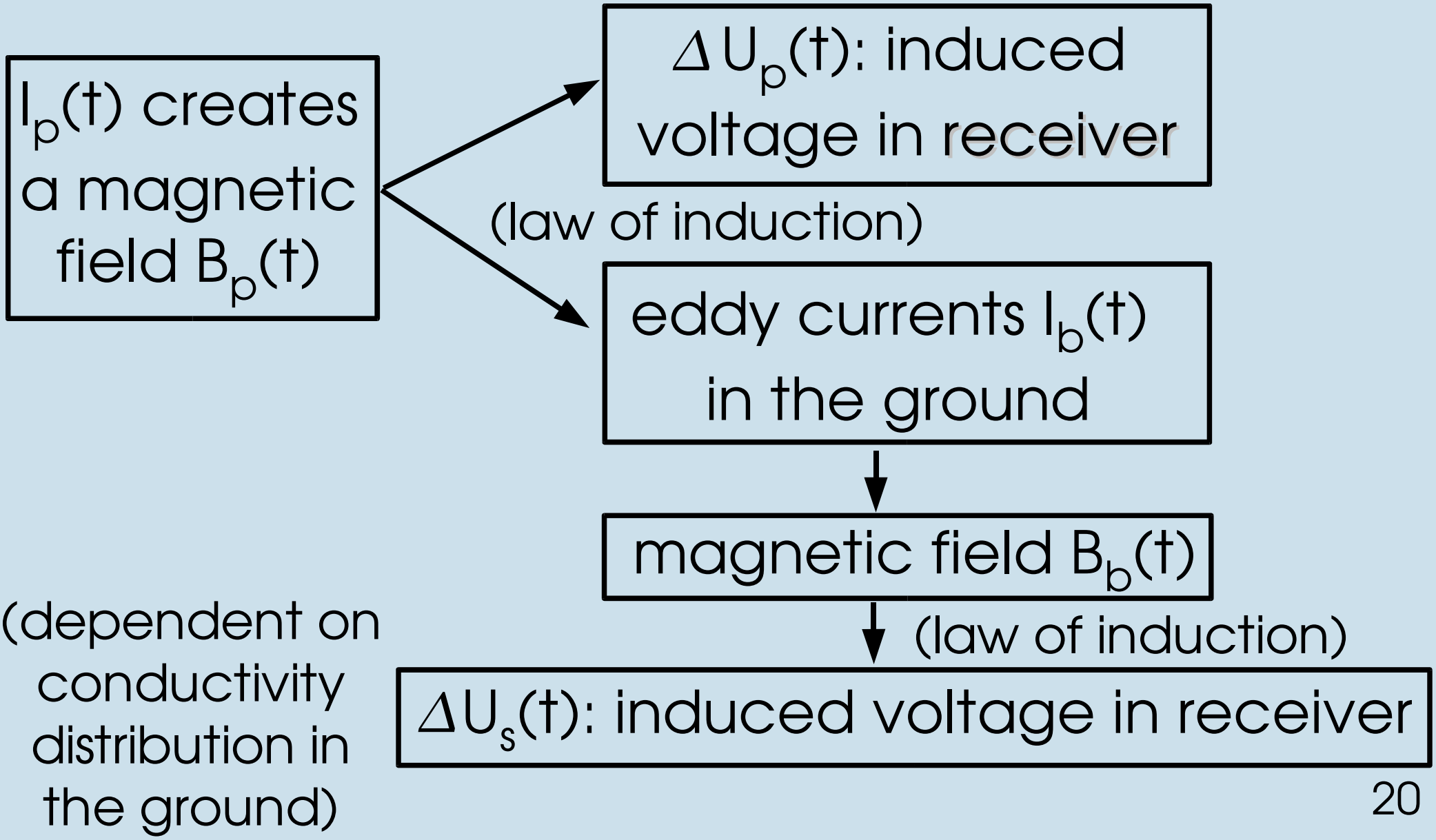

3.4.1 Signal decomposition

Induced currents and the associated secondary magnetic fields differ in phase from the primary field, and detected signals can therefore be resolved into components which are in phase and 90° out of phase with the primary field.

In phase components sometimes termed as real, as opposed to imaginary, quadrature or simply out of phase.

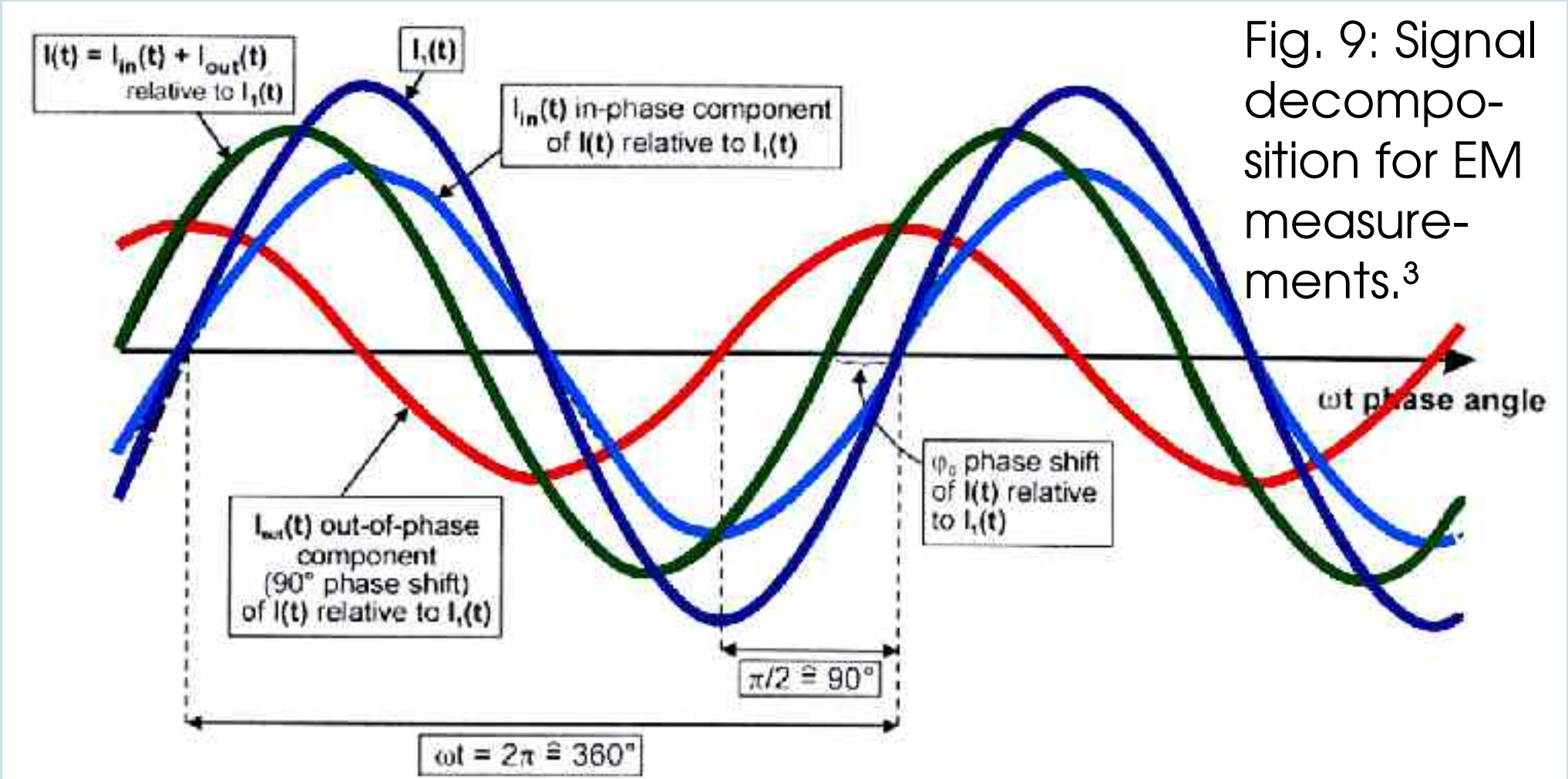

Fig. 9: Signal decomposition for EM measurements.[3]

current in the transmitter coil (induced signal) $I_1(t) = I_0 \sin(\omega t)$

current in the receiver coil (recorded signal) $I(t) = I_0 \sin(\omega t + \phi_0) = I_{in}(t) + I_{out}(t)$

out-phase (90°-phase) signal ("imaginary part", Im) $I_{out}(t)$

in-phase (0°-phase) signal ("real part", Re) $I_{in}(t)$

Signal decomposition

measured signal at receiver:

$$\Delta U_s(t) + \underbrace{\Delta U_p(t)}_{\text{can be eliminated}}$$

result: - amplitude of the 0°-phase and 90°-phase of $\Delta U_s(t)$
- phase shift of $\Delta U_s(t)$ relative to $\Delta U_p(t)$

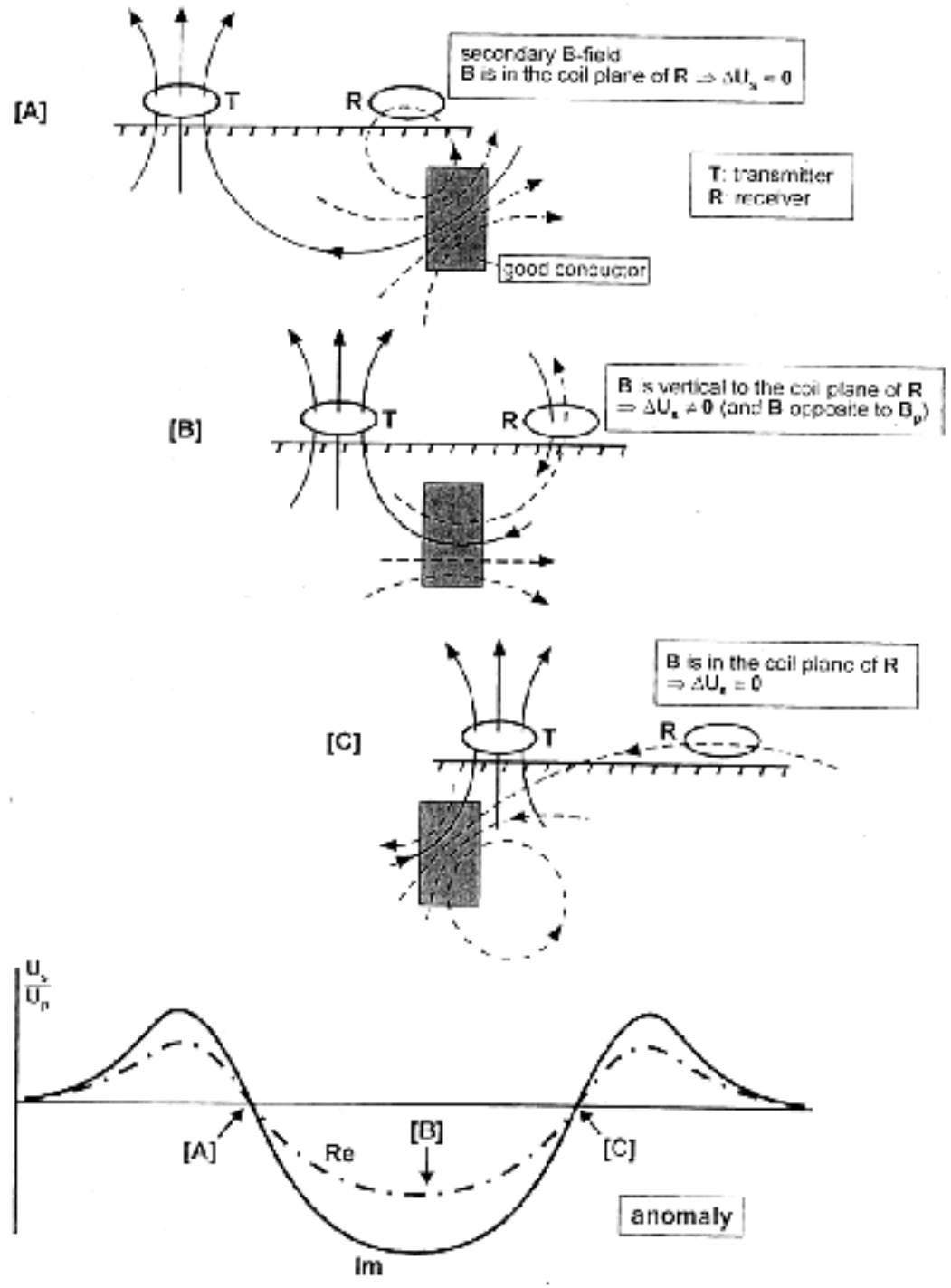

Fig. 10: Explanation of Slingram anomaly [3]

3.4.2 The Slingram anomaly

No anomaly is detected by a horizontal receiving coil immediately above the body because the secondary field there is horizontal.

Similarly there will be zero anomaly when the transmitter coil is vertical above the body because no significant eddy currents will be induced.

The greatest (negative) secondary field values will be observed when the conductor lies mid-way between the two coils.

3.4.3 Airborne Systems

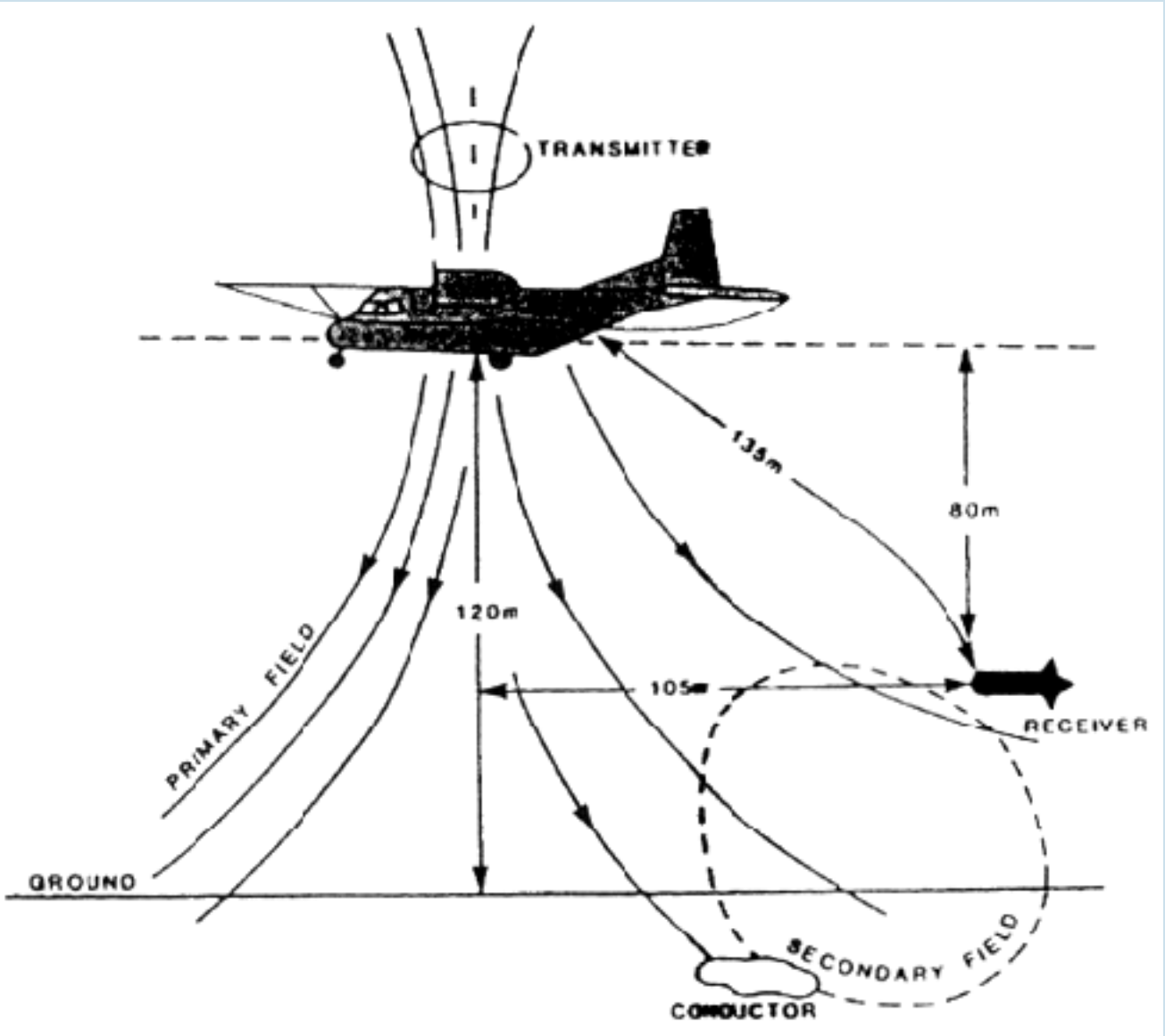

Fig. 11: Principle of airborne electromagnetic surveying. The system shown deployed is of the towed-bird type.[1]

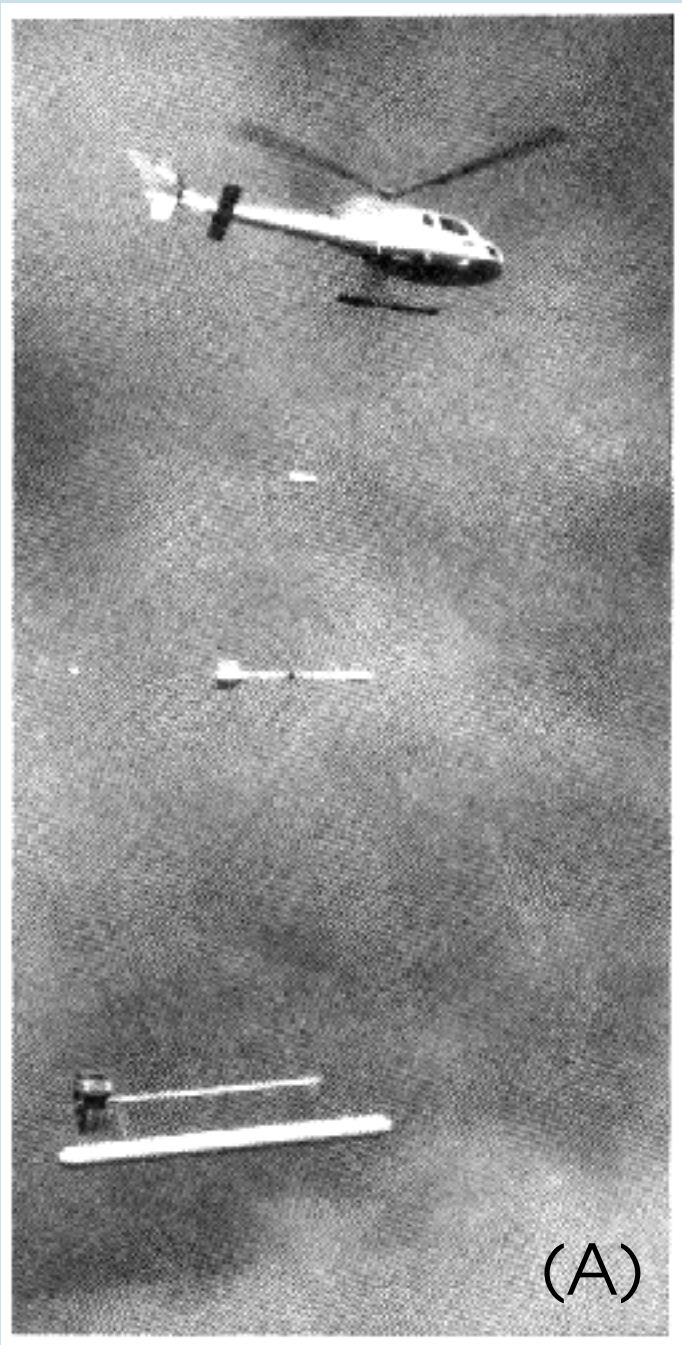

Fig. 12: (A) Eurocopter AS350B towing three instrument pods. They are from the top 2-channel VLF-EM, total-field cesium magnetometer, and a 5-frequency electromagnetic induction system. (B) Cessna 404 fixed wing aircraft with a total field magneto-meter mounted in a tail stinger.[1]

3.4.4 Case histories

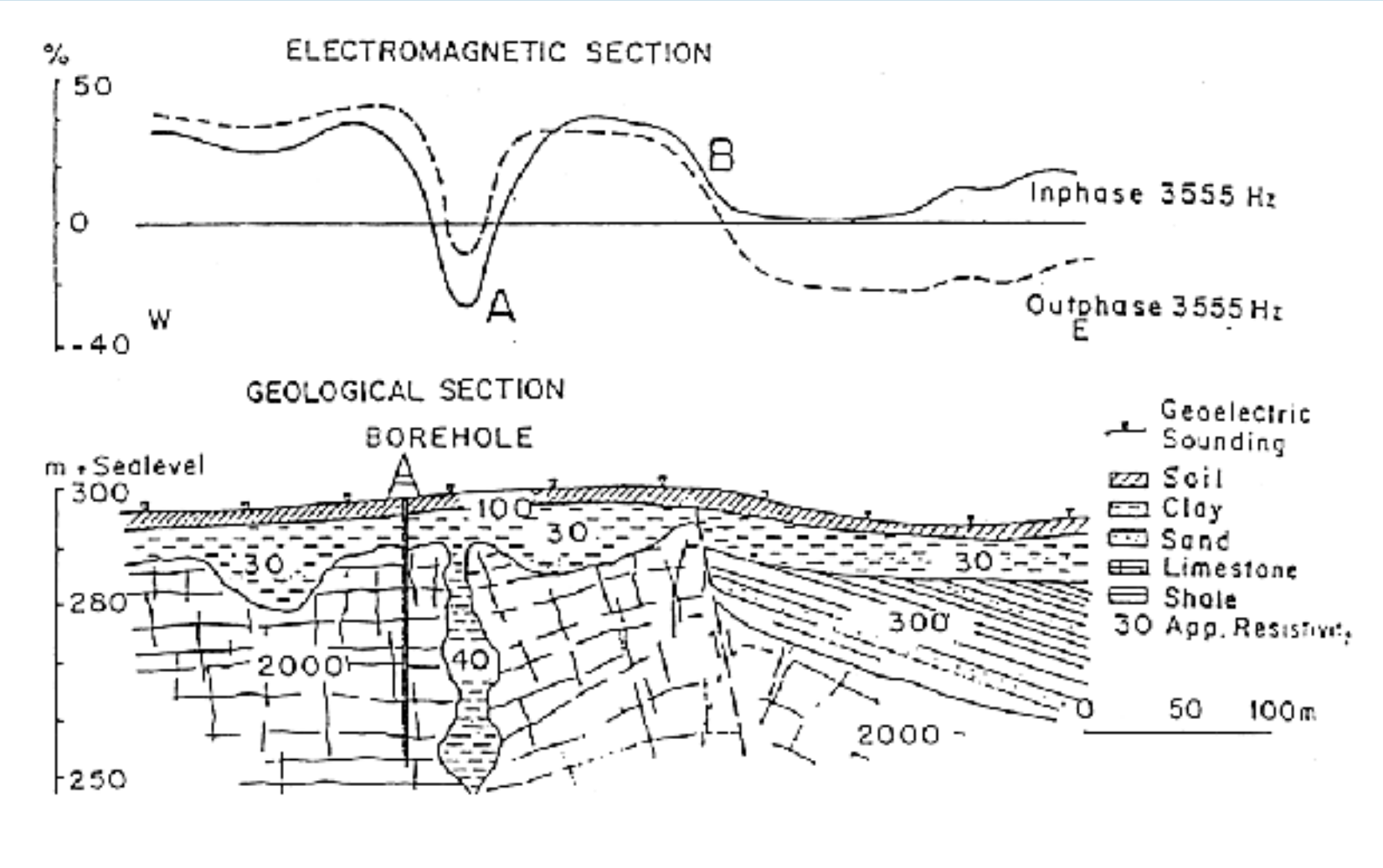

Fig. 13: Mapping using electromagnetic induction. [4]

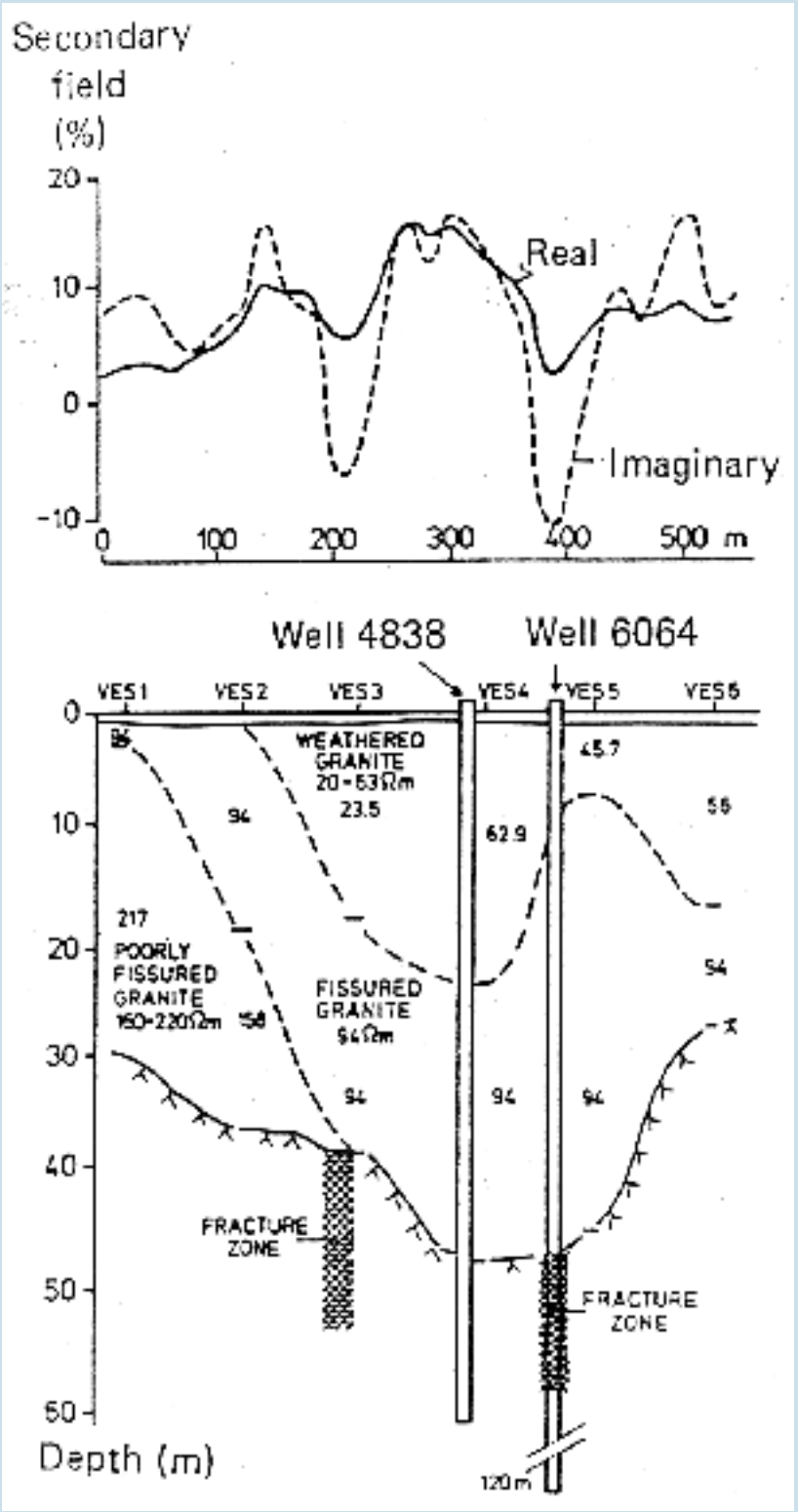

Fig. 14: EMAC 36 results and geological section, Modipane, Botswana.

3.4.5 Ground conductivity meters (measurements at low induction number)

The instruments (manufactured by Geonics Ltd.) provides a direct reading of the quadrature as the apparent conductivity in mS/m.

The secondary EM field measured in a mobile transmitter receiver system is generally a complex function of the coil spacing s, the operating frequency f and conductivity of the subsurface σ .

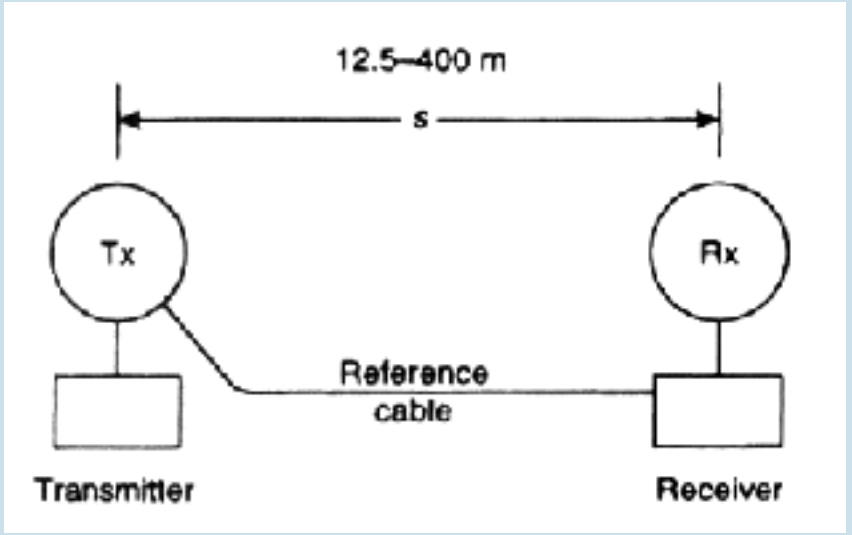

Fig. 15: Moving dual-coil EM system; circles indicate the transmitter (Tx) and receiver (Rx) coils.[1]

Ground conductivity meters

The ratio of the intercoil spacing (s) divided by the skin depth is known as the induction number B.

Where the induction number is less than one, then the ration of the secondary to the primary of magnetic fields at the receiver is directly proportional to apparent conductivity.

The ratio of the secondary (H_s) to primary (H_p) magnetic fields at the receiver at low induction numbers (B<<1) is given by

$$H_s/H_p = i\omega\mu_0 s^2/4$$

Ground conductivity meters

The measuring system is designed to ensure that with the selected frequency f, for a given inter-coil separation (s), a designed response of H_p for a given transmitter, the only unknowns H_s which is measured by the instrument

$$\sigma_a = (4/\mu_0 \omega s^2)(H_s/H_p)_q$$

where the subscript q denotes the quadrature phase.

Two devices: EM31 and EM 34-3

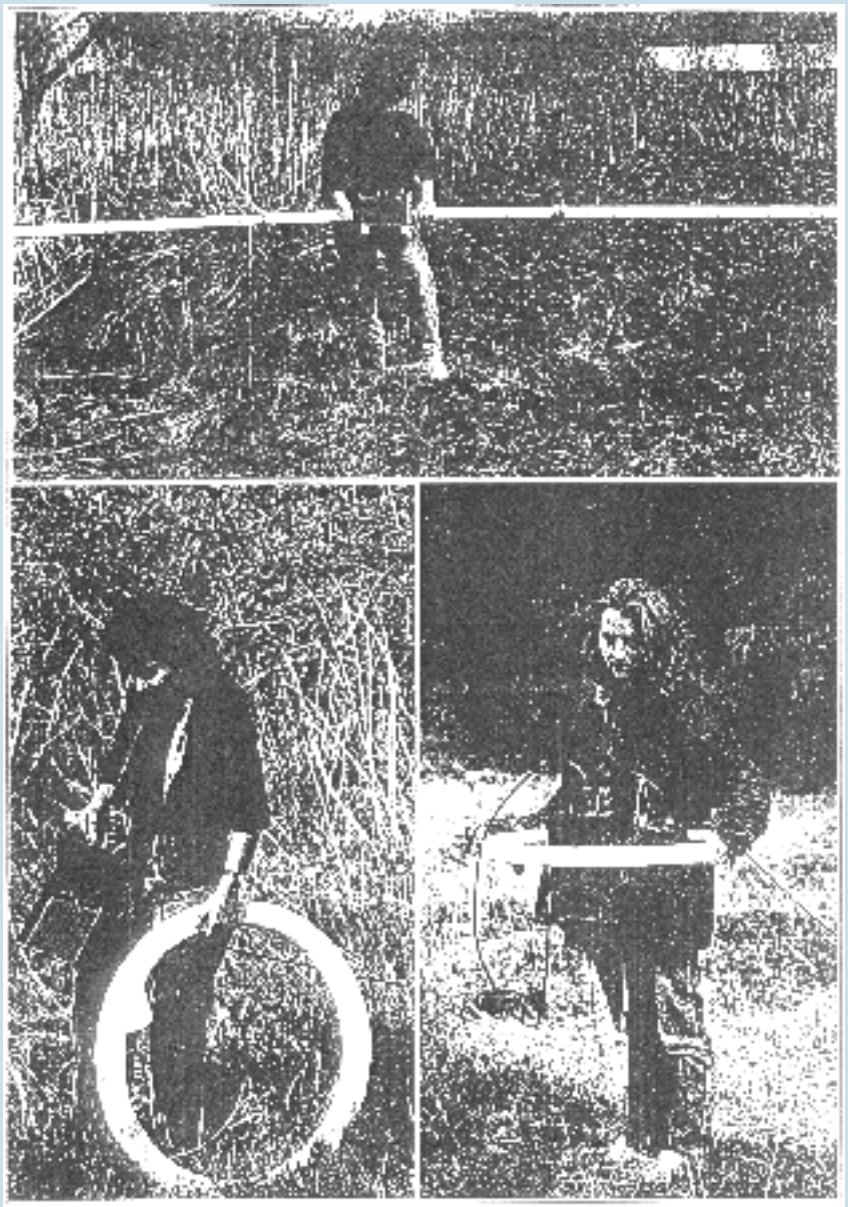

EM 31:

3.7 m coil spacing f=9.8 kHz

EM 34-3:

10 m coil spacing f=6.4 kHz

20 m coil spacing f=1.6 kHz

30 m coil spacing f=0.4 kHz

Fig. 16

3.4.5.1 Case histories

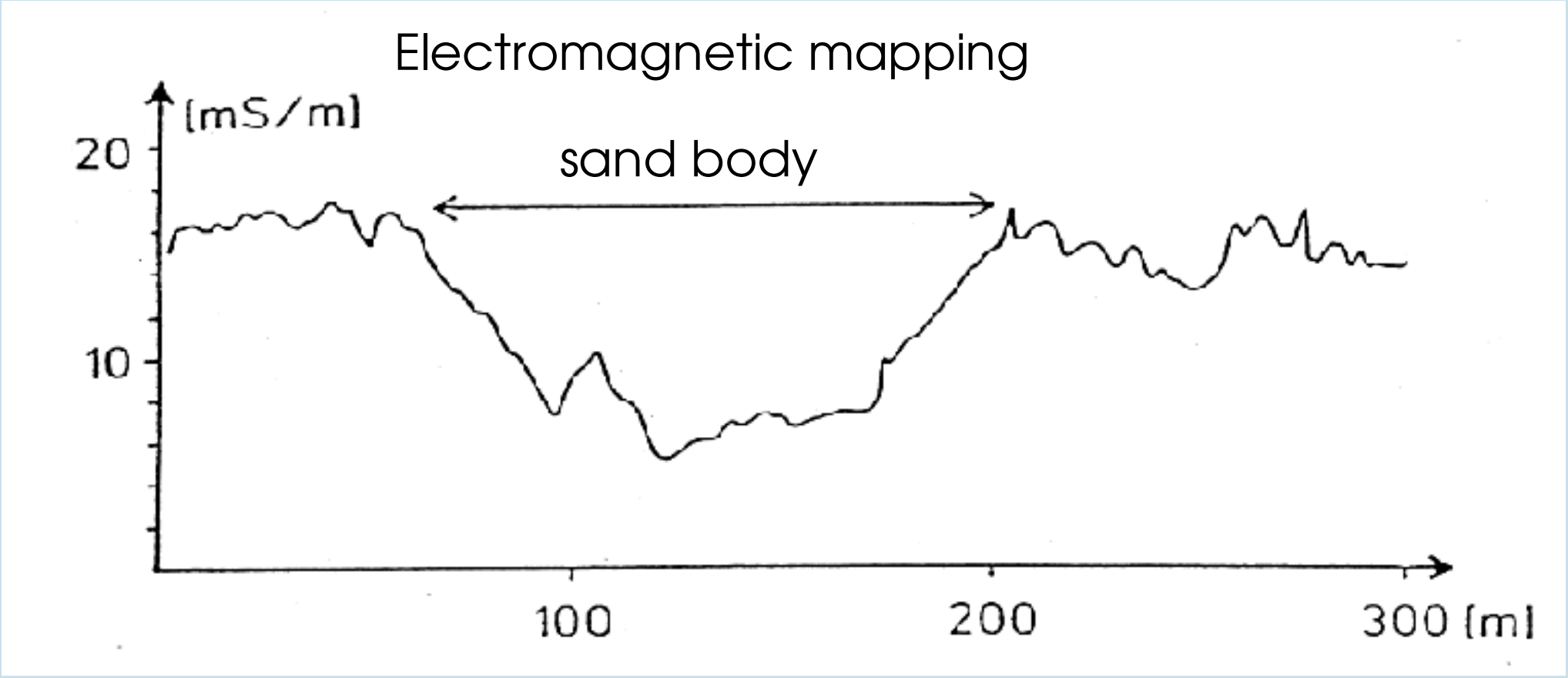

Fig. 17: Mapping lateral changes of the near-surface geology with electromagnetic methods. A sand body causes a decrease in conductivity.

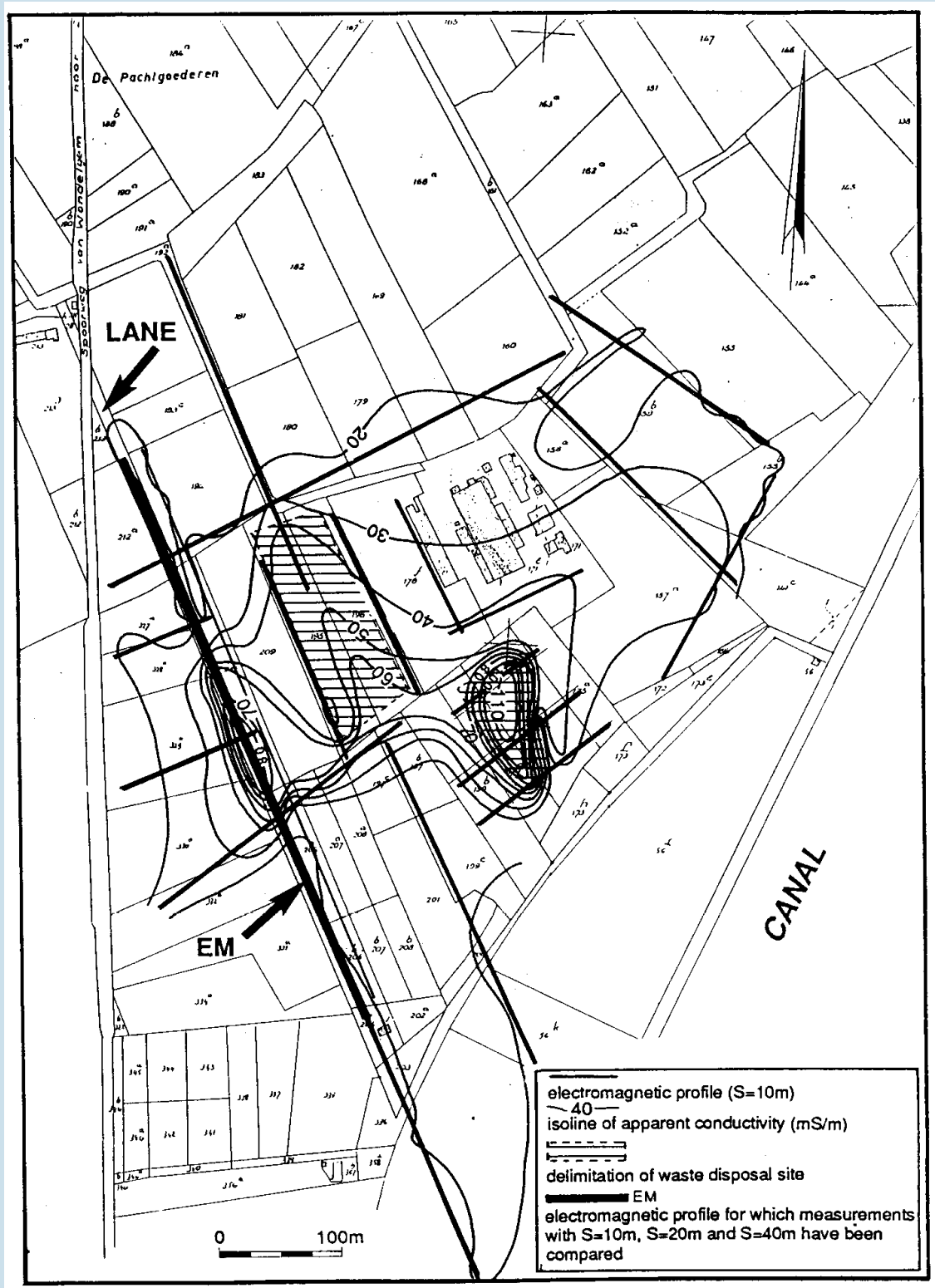

Fig. 18: Contours of apparent conductivity for EM34 measurements with an intercoil spacing of 10m at two waste sites in Belgium. [5]

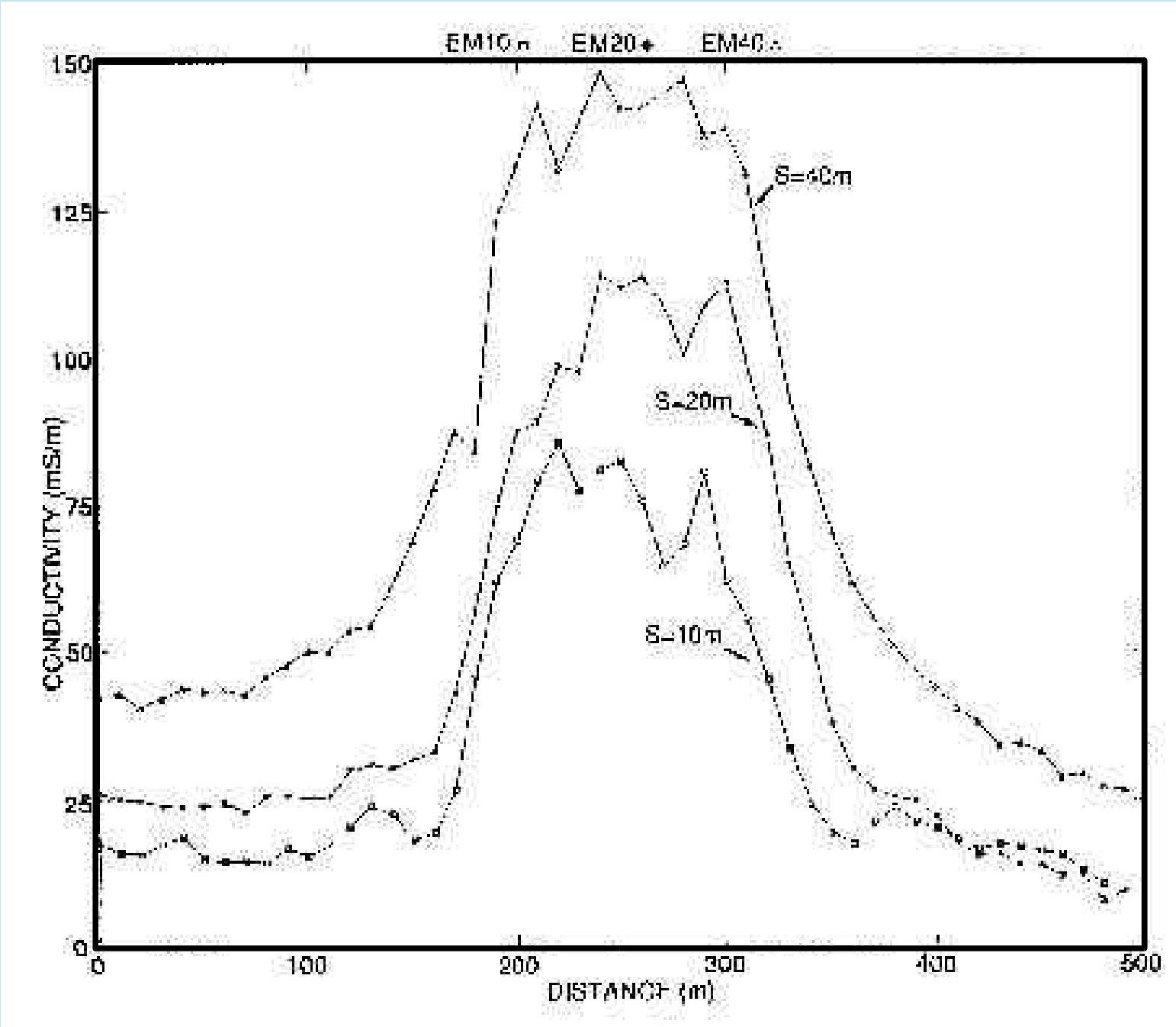

Fig. 19: EM34 measurements with an intercoil spacing of 10, 20 and 40m along the lane indicated in figure 17. [5]

3.5 The Very Low Frequency (VLF) method

Slingram and ground conductivity meters are near field methods. VLF technique is a far field method.

The source of the VLF method is electro-magnetic radiation generated in the low-frequency band of 15-25 kHz by the powerful radio transmitters used in long-range communication and navigational systems.

There are more than a score of stations around the world transmitting VLF signals continuously for military purposes.

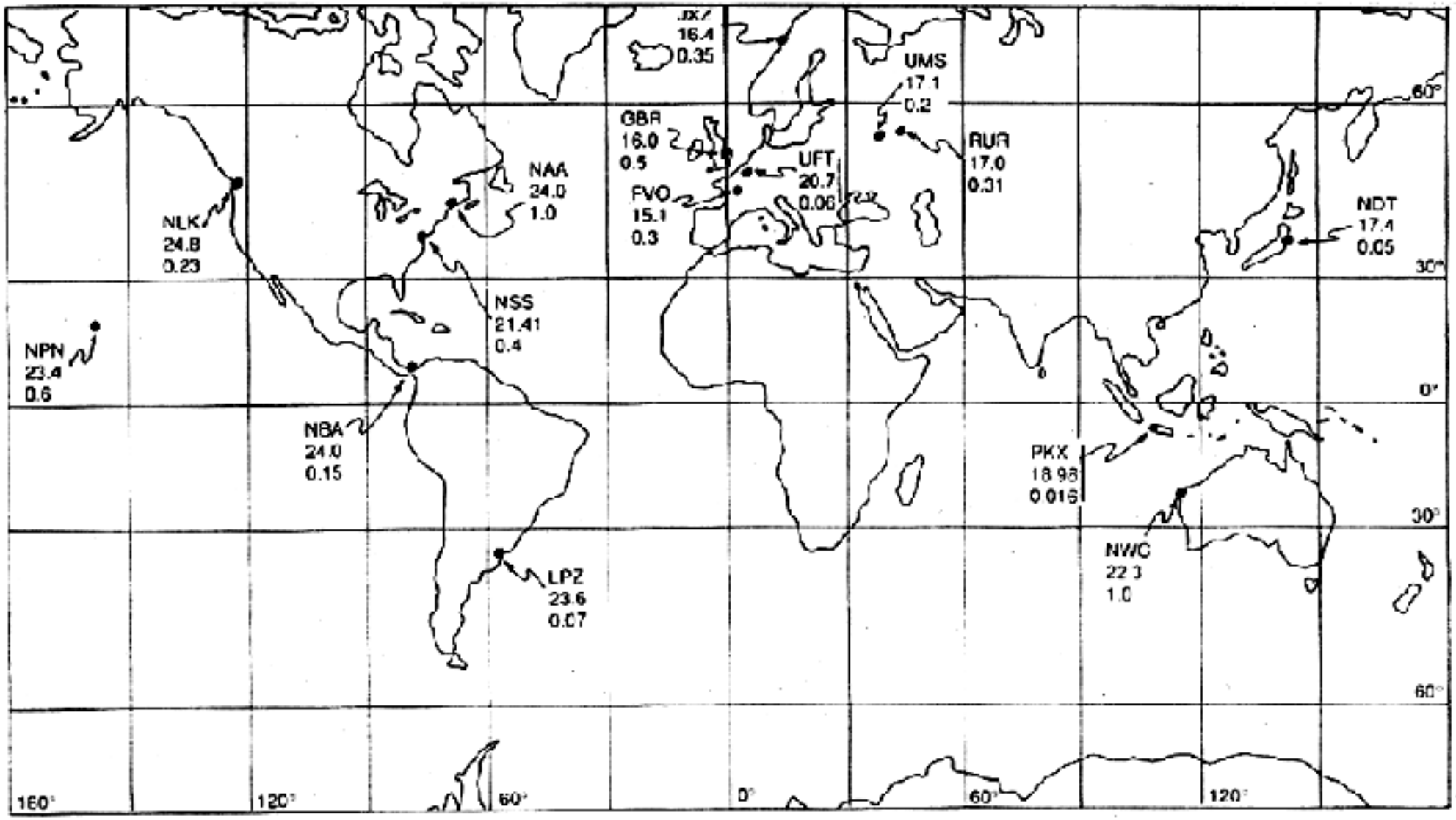

Fig. 20: Major VLF transmitters. Data blocks identify station codes (e.g. NAA), frequencies in kHz and power in megawatts. Frequencies and powers are liable to change without much notification. [6]

The Very Low Frequency (VLF) method

Signal level contours for two of the major VLF-transmitters are shown in the following figure.

Areas enclosed with the 54 dB contours have good signal strengths while those with 48 dB contours have marginal signal strength.

Areas left unshaded have signal strength too weak for the method.

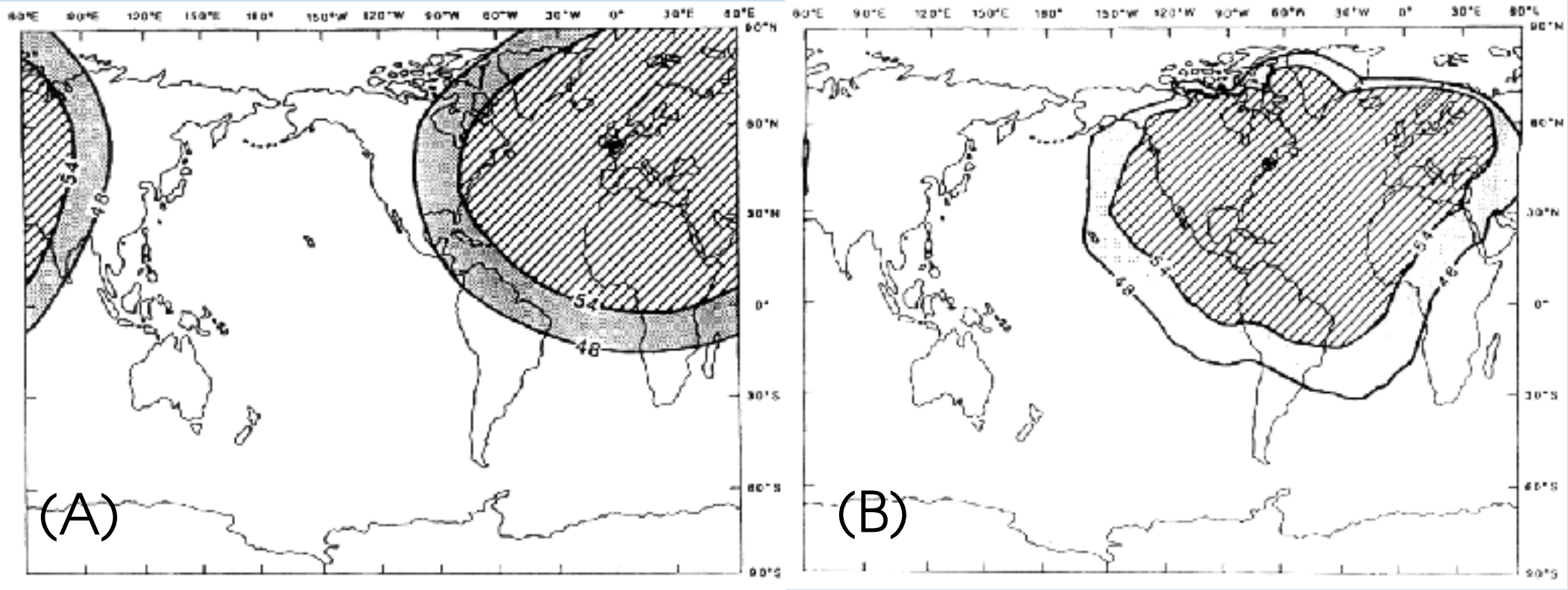

Fig. 21: Signal level contours for VLF transmitters at (A) GBR, Rugby, UK and (B) NOAA, Cutler, USA.[1]

Wave propagation at VLF frequencies

Waves at VLF frequencies propagate efficiently over long distances in the wave guide formed by the ground surface and the ionosphere.

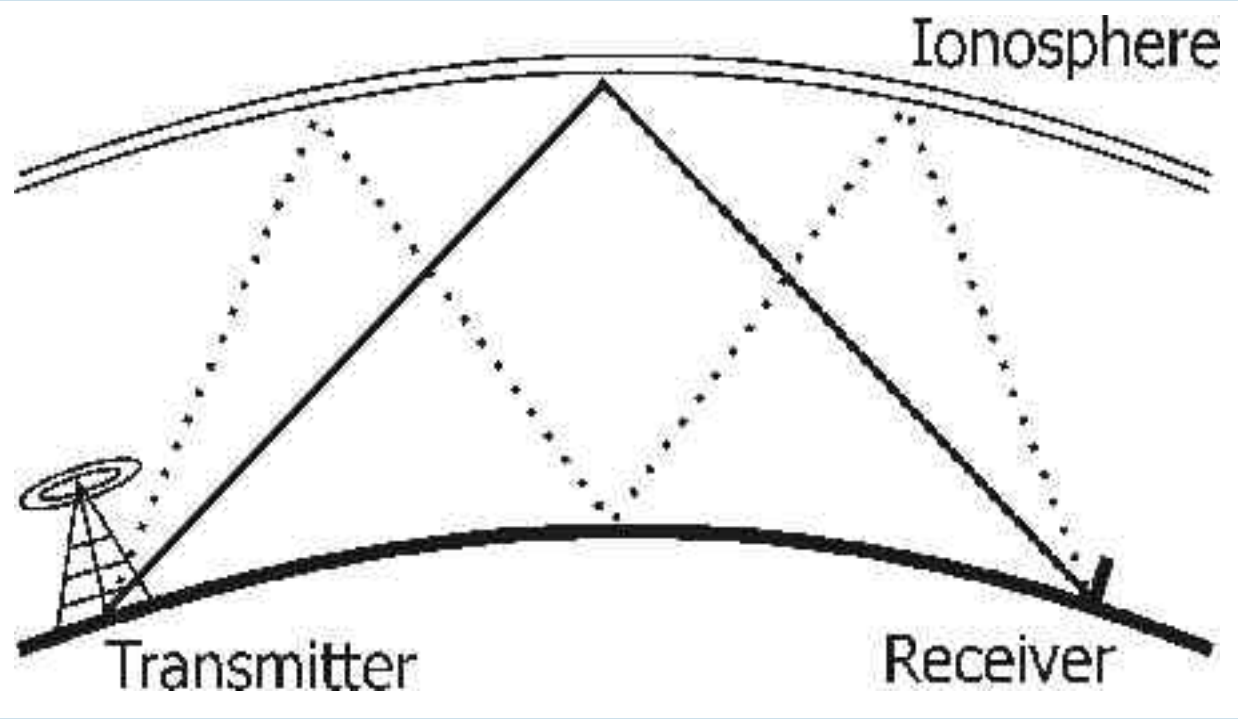

Such signals may be used for surveying up to distances of several thousand kilometers from the transmitter.

Fig. 22

Principle of the VLF method

At large distances from the source the EM-field is essentially planar and horizontal.

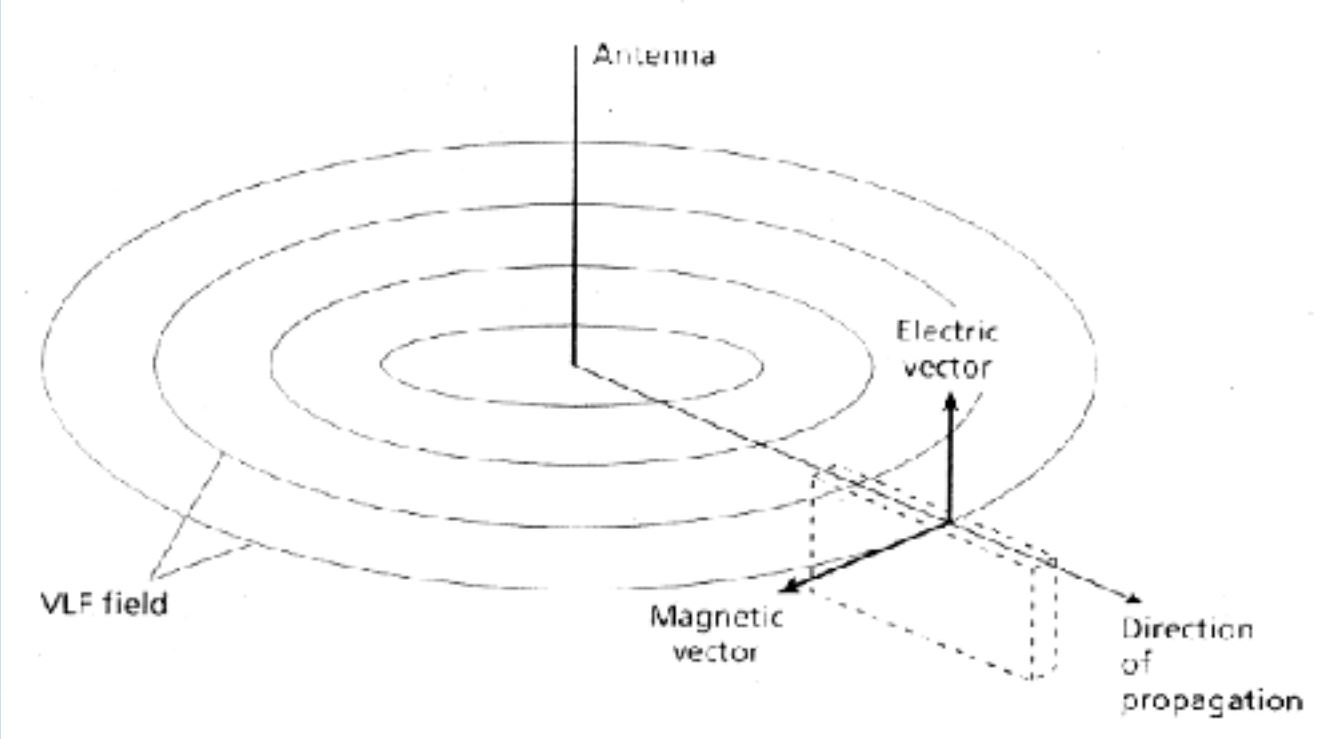

Fig. 23: Principle of VLF method. Dashed lines show a tabular conductor striking towards the antenna which is cut by the magnetic vector of the EM field.[2]

Electric and magnetic field

The electric component E lies in a vertical plane and the magnetic component H lies at right angles to the direction of propagation in a horizontal plane.

A conductor that strikes in the direction of the transmitter is cut by the magnetic vector and the induced currents produce a secondary magnetic field

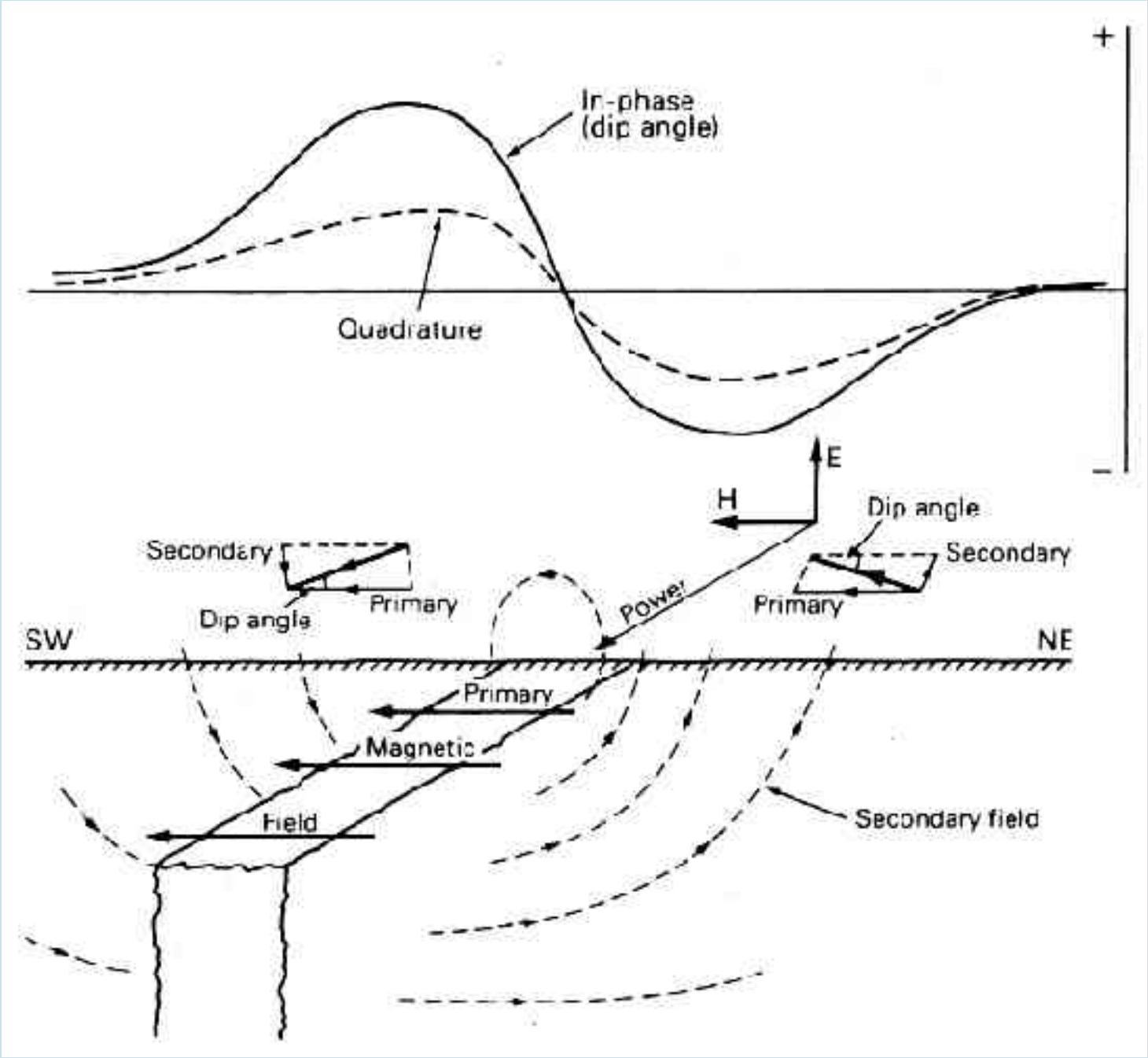

Fig. 24: Magnetic component anomaly over a vertical conducting sheet striking towards the transmitter. Note the need of a sign convention.[6]

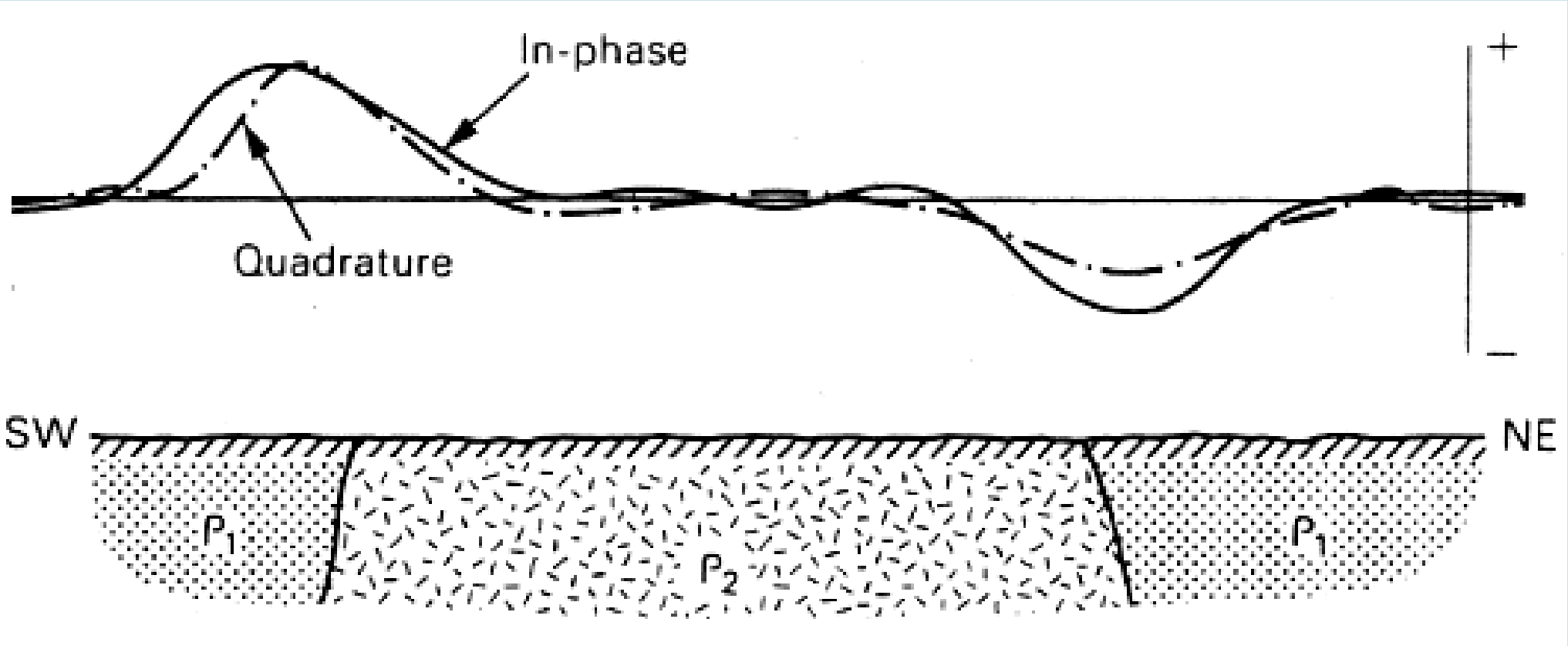

Fig. 25: VLF magnetic field anomalies at the margins of an extended conductor.[6]

Field equipment

The field equipment is small and light, conventionally operated by one person.

There is no need for a transmitter.

<u>Disadvantages:</u> For a particular survey area there may be no suitable transmitter producing a magnetic vector across the strike. Penetration depth is somewhat less than Slingram methods.

3.5.1 Case histories

Fig. 26: Car-borne VLF measurements. [5]

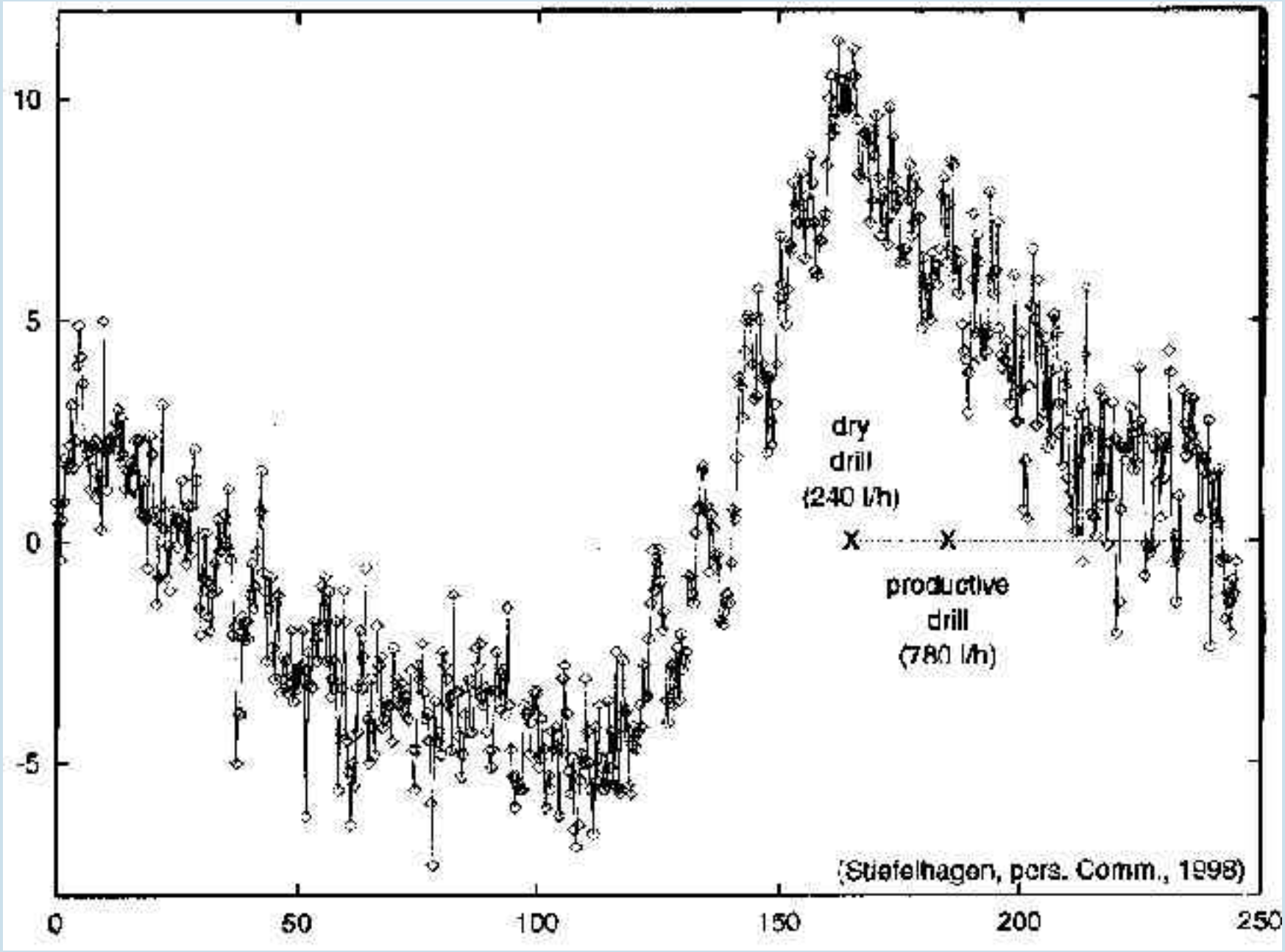

Fig. 27: VLF data (out of phase component) on a profile for groundwater exploration in Niger. The frequency used was 18.3 kHz. Borehole locations are also marked. [5]

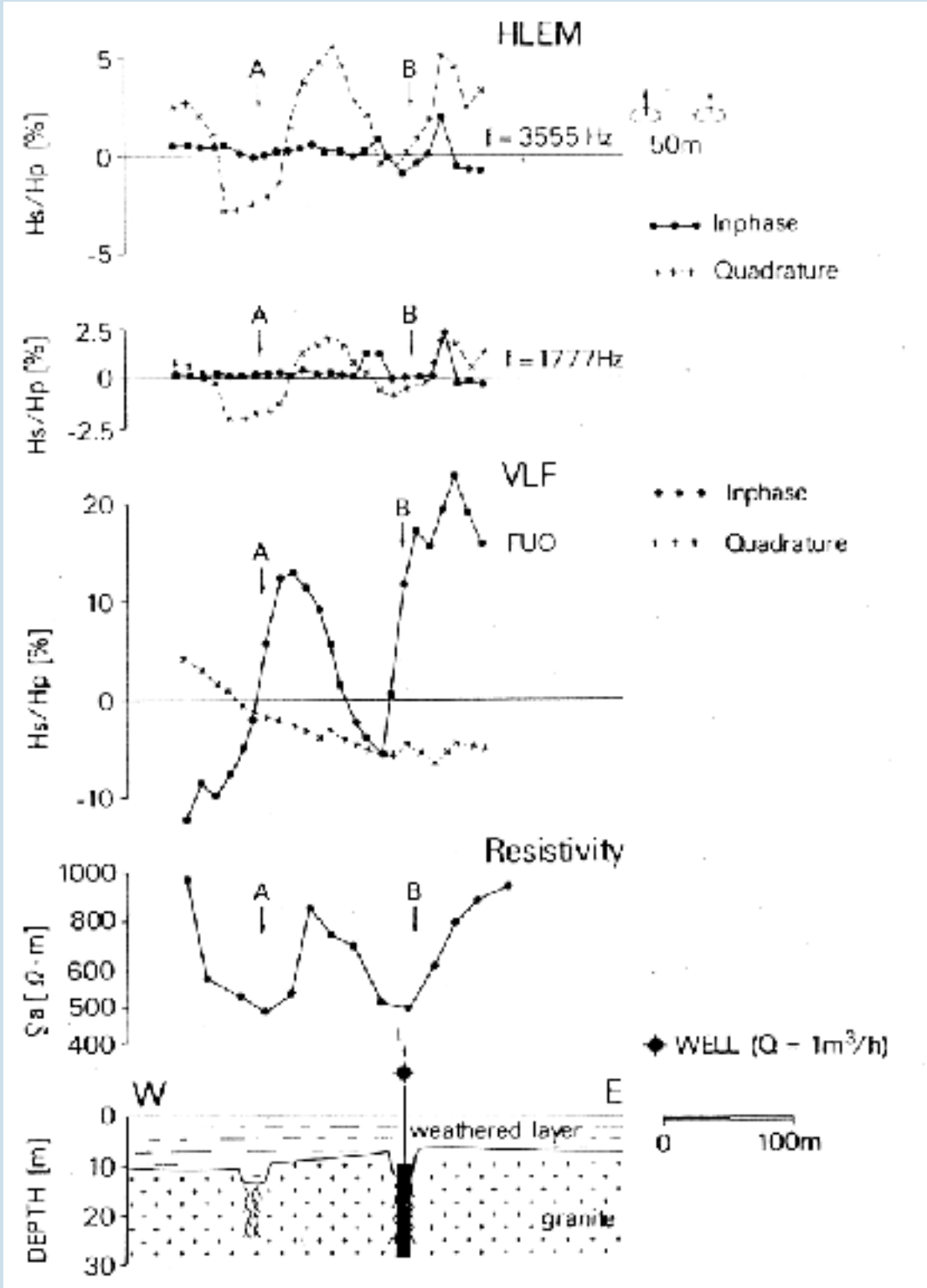

Fig. 28: Comparison of VLF and other electromagnetic and electric data over granite and volcano sedimentary rocks in Burkina Faso, Africa. [4]

3.6 The radiomagneto-telluric method (RMT)

The RMT technique uses as transmitters military and civilian radio stations broadcasting in a frequency range between 10 kHz and 1 MHz.

The electromagnetic waves radiated from these transmitters into the conductive earth induce current systems which are connected with electrical and magnetic alternating fields.

The magnetic field can be measured by a coil (0.4 m diameter) and the electric field by two grounded electrodes. The distance between two electrodes can be chosen as 1 or 5 m.

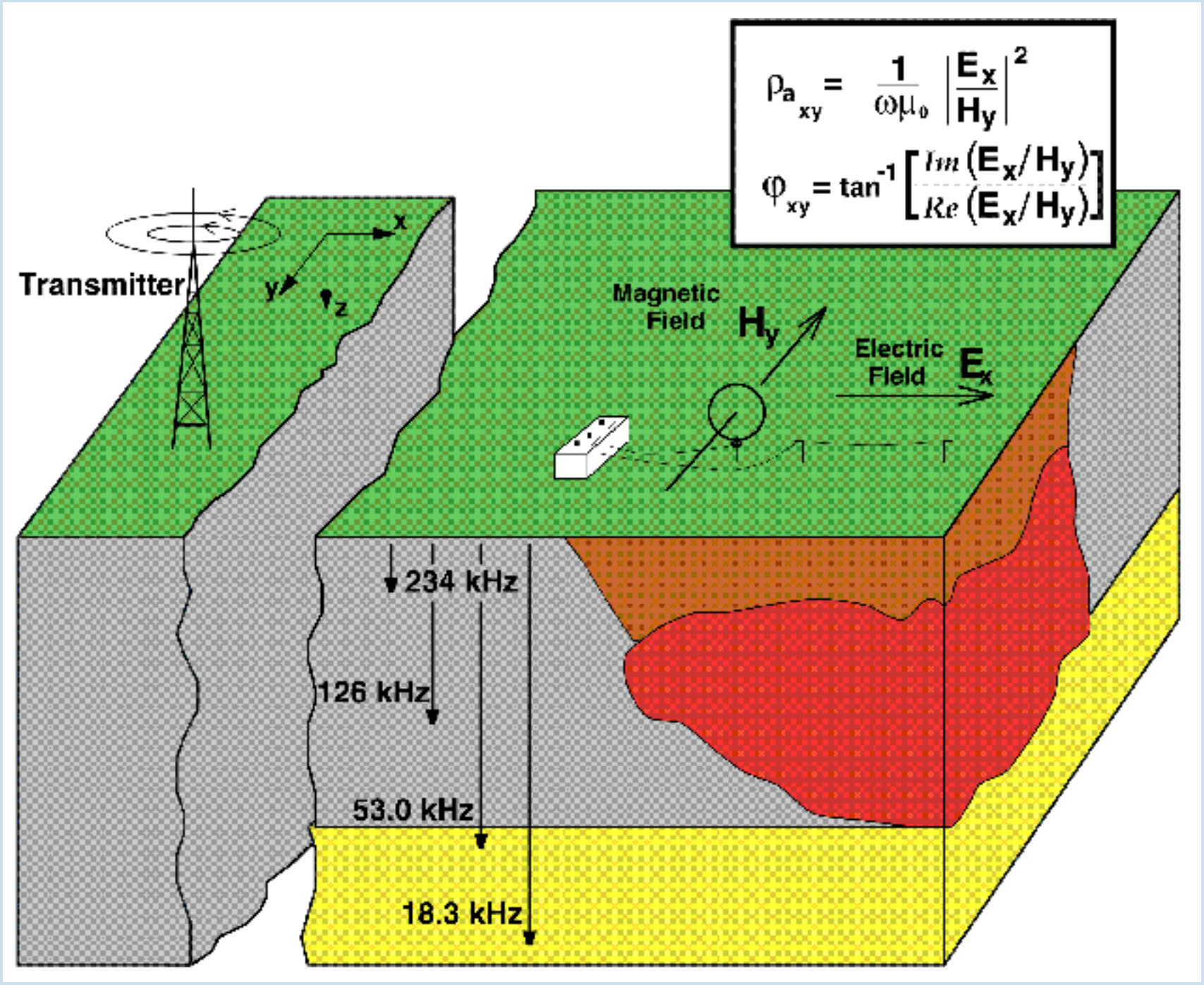

Fig. 29: Schematic diagram illustrating a RMT field setup over a hazardous waste site. [5]

The measuring device only weighs 7 kg and about 3 minutes are are required for measuring four frequencies at one station.

Fig. 30: RMT in the field.

Apparent resistivity and phase data

For the selected frequencies apparent resistivity and phase data can be derived from the measured electric and magnetic field.

$$\rho_a(f) = \frac{1}{2\pi\mu_0 f}\left|\frac{E_x}{H_y}\right|^2 \qquad \phi(f) = \tan^{-1}\left[\frac{\Im(E_x/H_y)}{\Re(E_x/H_y)}\right]$$

Plot apparent resistivity and phase as a function of frequency.

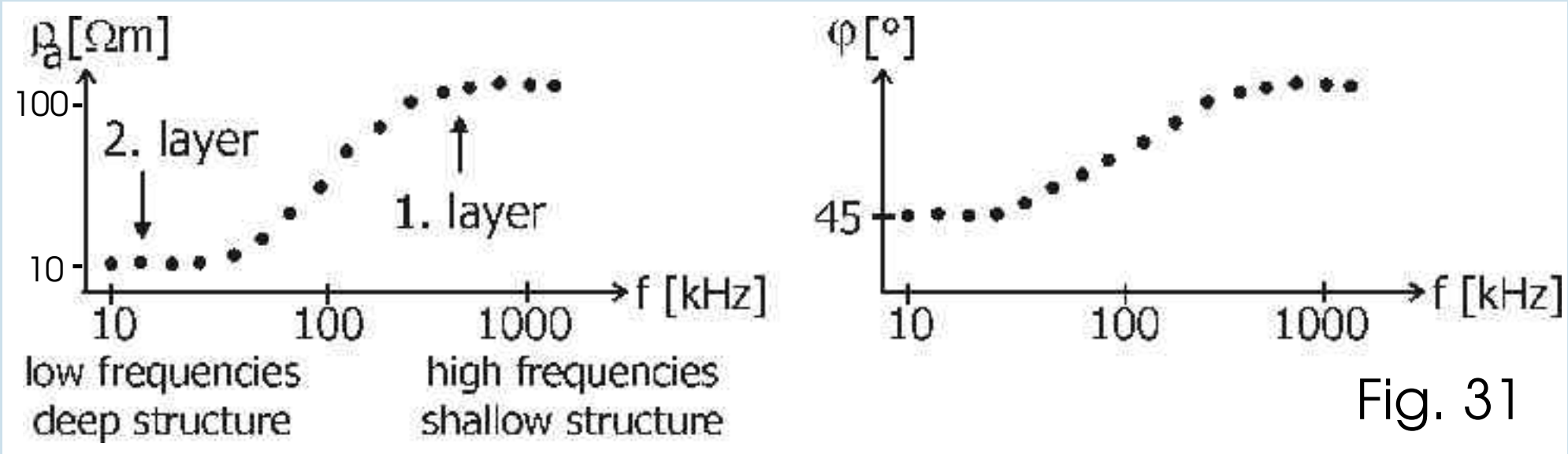

Fig. 31

Interpretation of phase

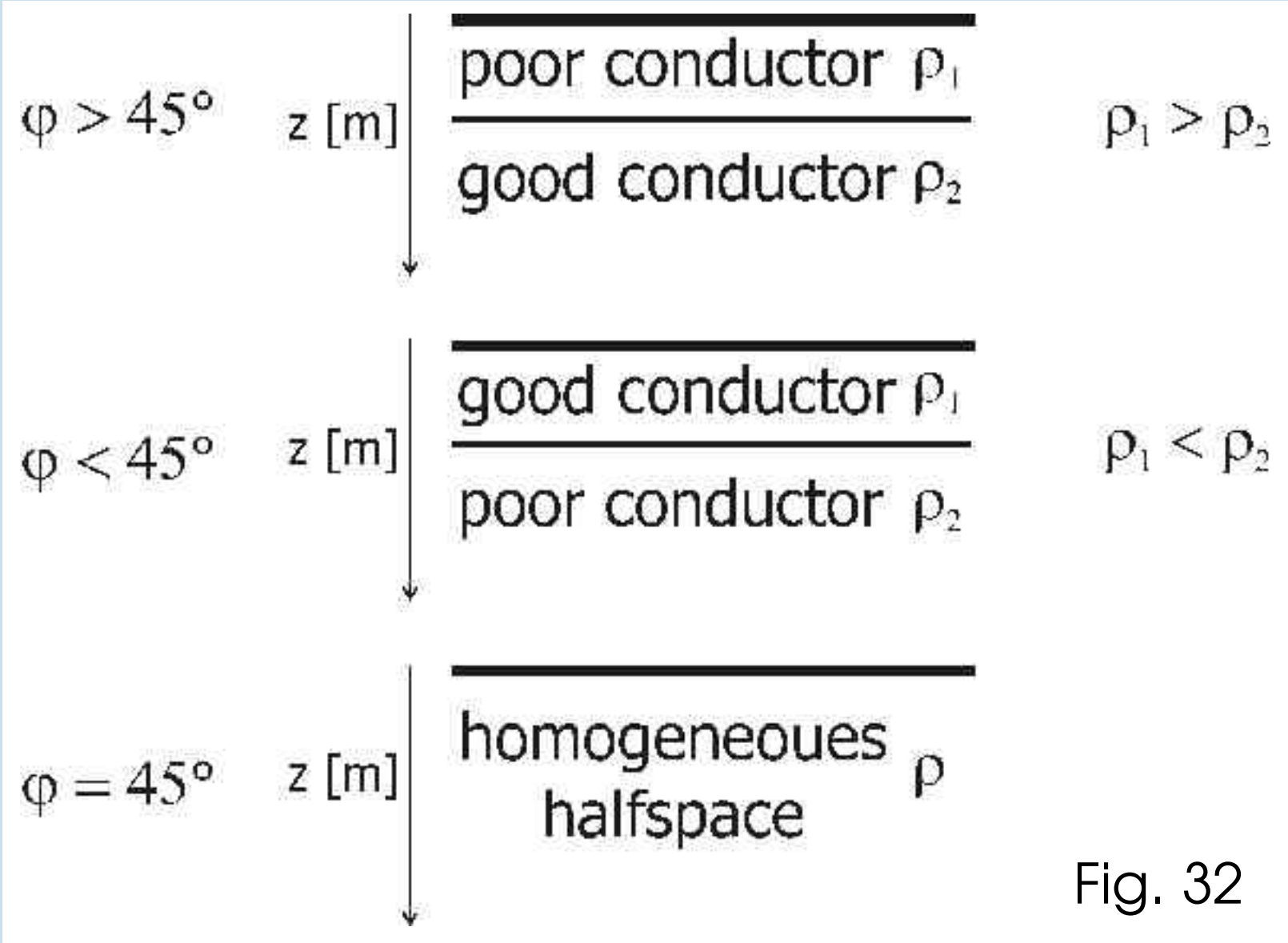

Fig. 32

3.6.1 RMT surveys

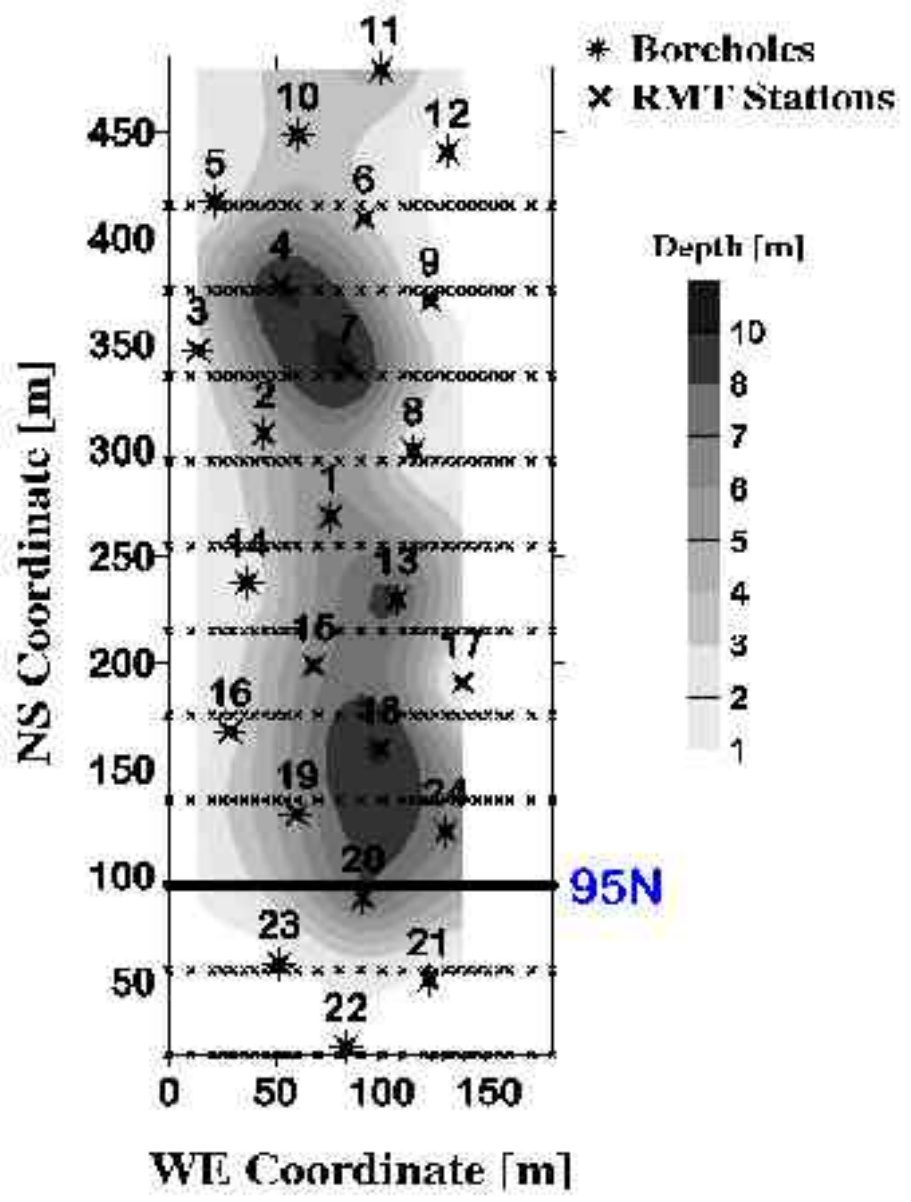

Fig. 33: Lower boundary derived from drillings of a waste site near Cologne.[5]

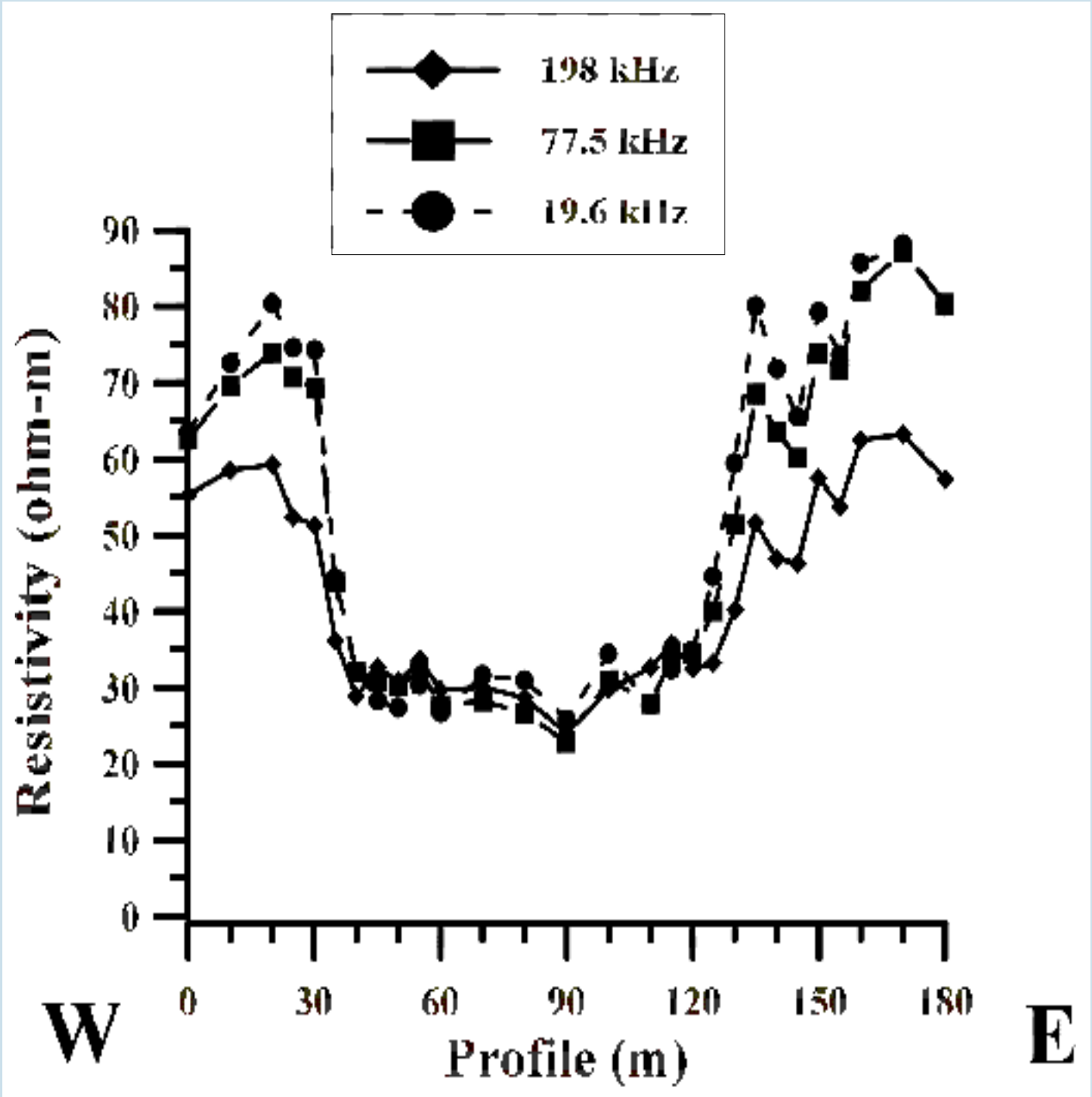

Fig. 34: Apparent resistivity data on profile 95 N for 3 frequencies at the Cologne waste site. The lateral boundaries at profile meter 30 and 130 coincide with the drilling results (...). The transmitters are located in EW-direction.[5]

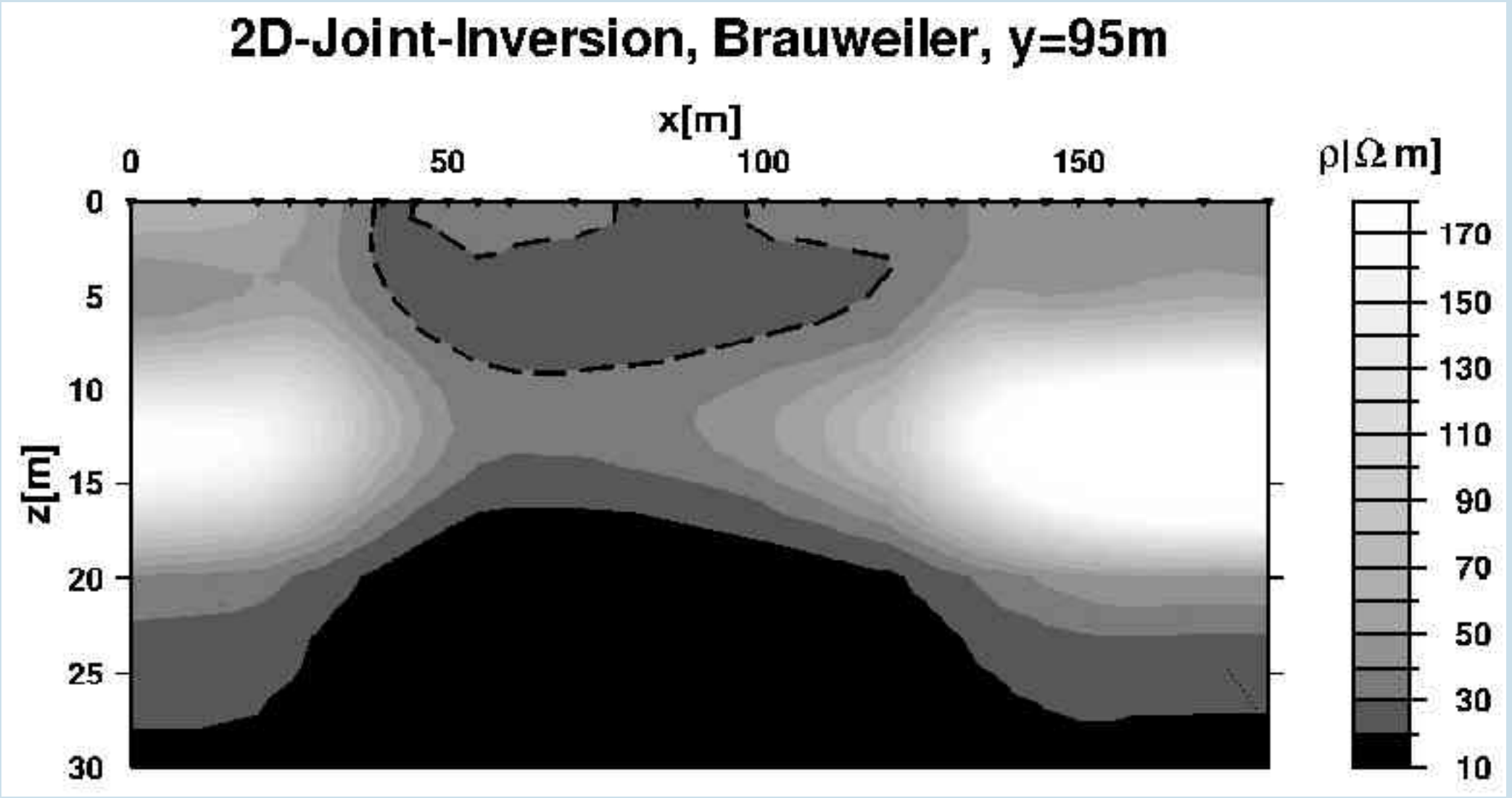

Fig. 35: 2D inversion result for profile 95N at the Cologne waste site which is characterized by low resistivities (<30 Ωm) between profile 30 and 120. The deeper low resistive structure indicates the clay layer.[5]

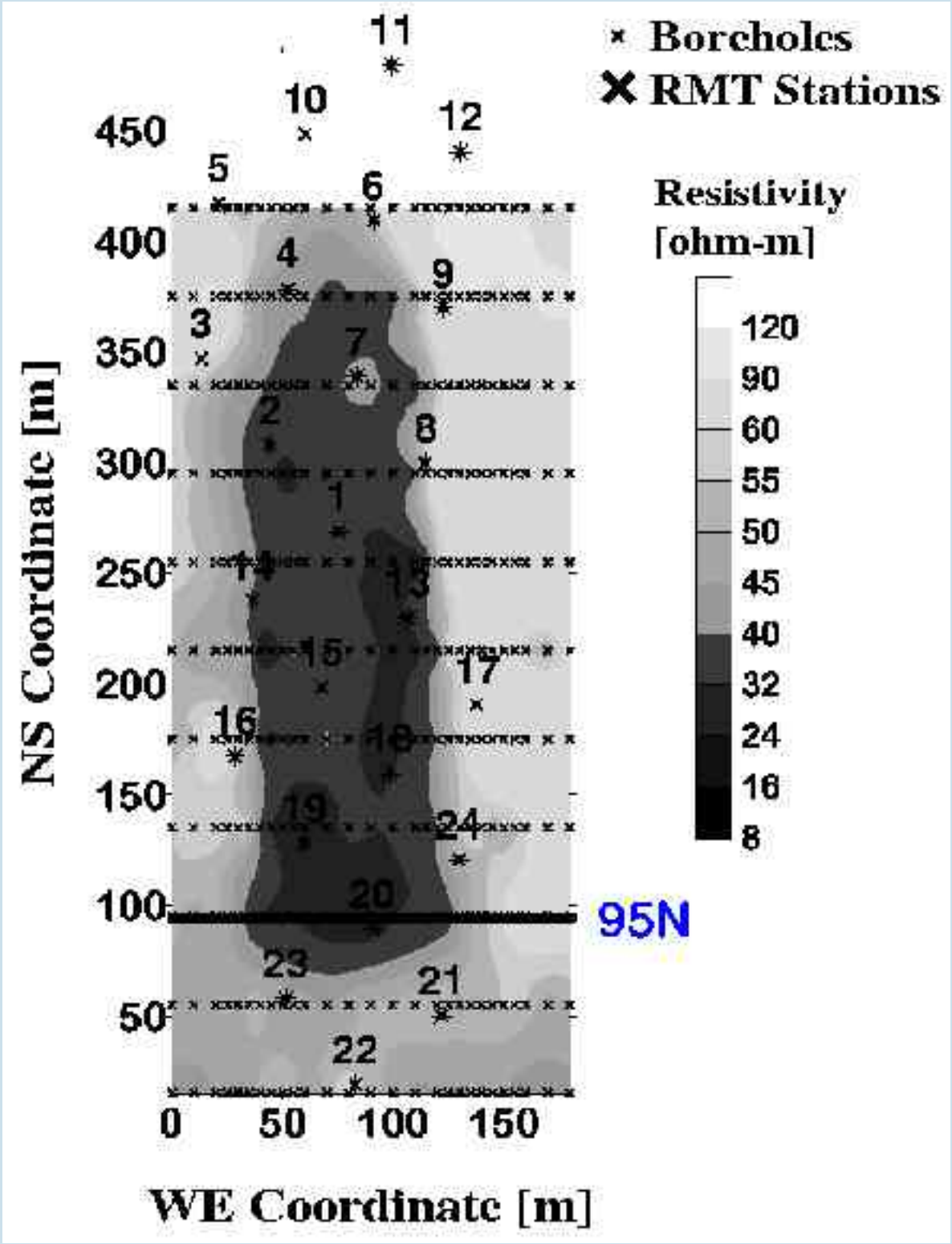

Fig. 36: Resistivity distribution of the survey area at 3m depth at the Cologne waste site.[5]

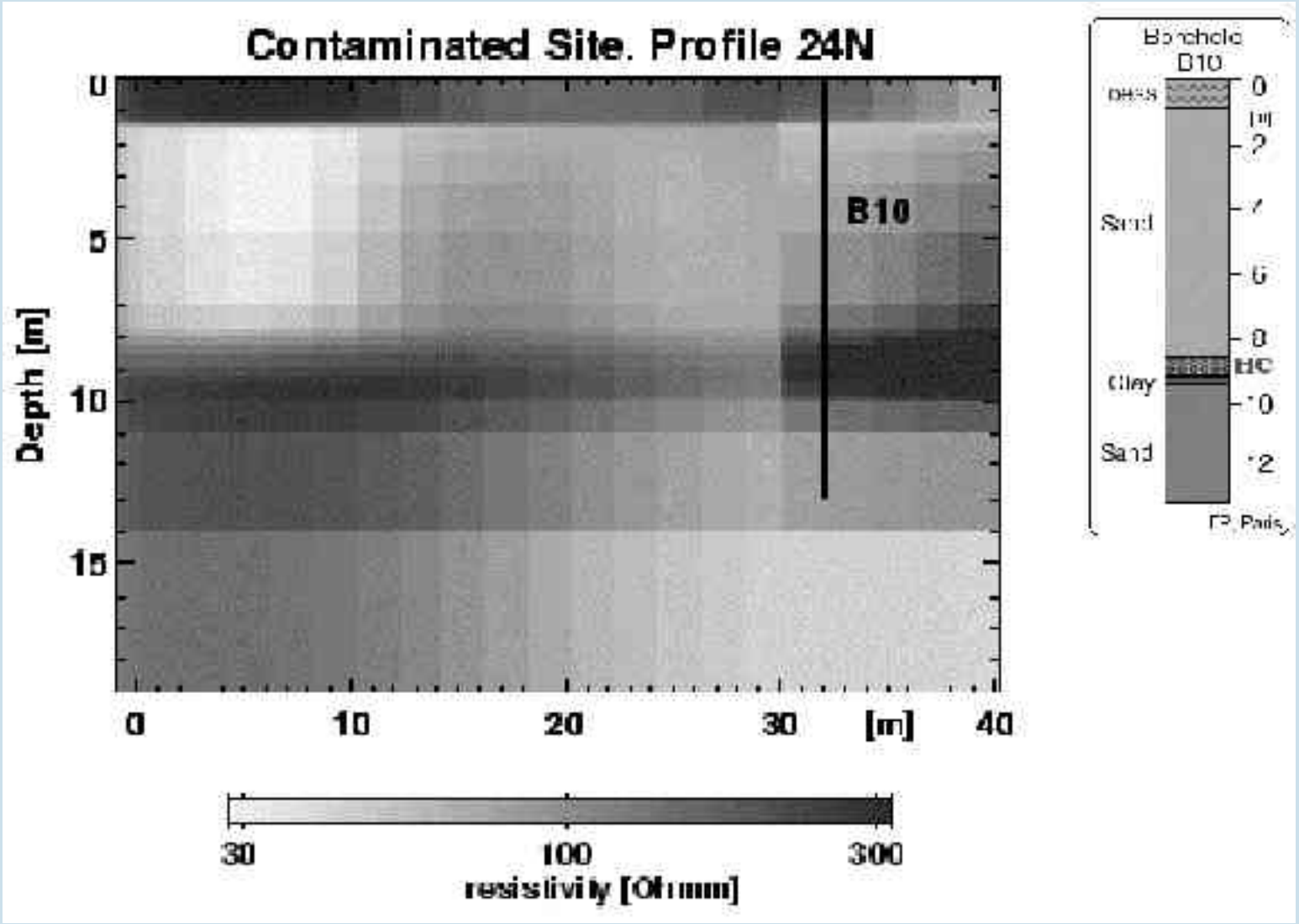

Fig. 37: A 2D conductivity model derived from RMT data observed on a profile at a contaminated site near the International Airport Strasbourg. The resistive layer at 9m depth may be interpreted as a contaminated zone in the sandy layer. [5]

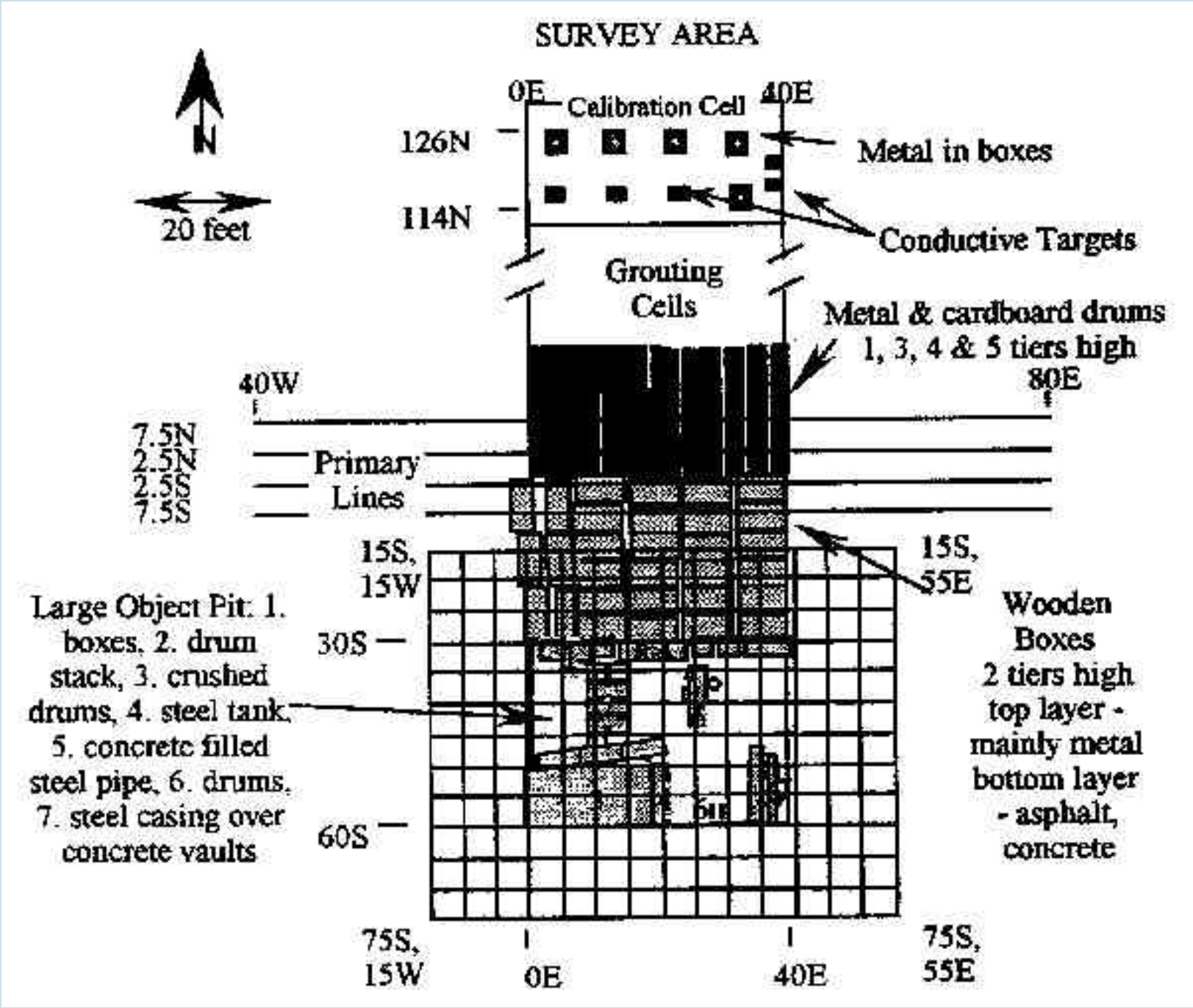

Fig. 38: Survey layout at the Idaho National Engineering Laboratory Cold Test Pit. [5]

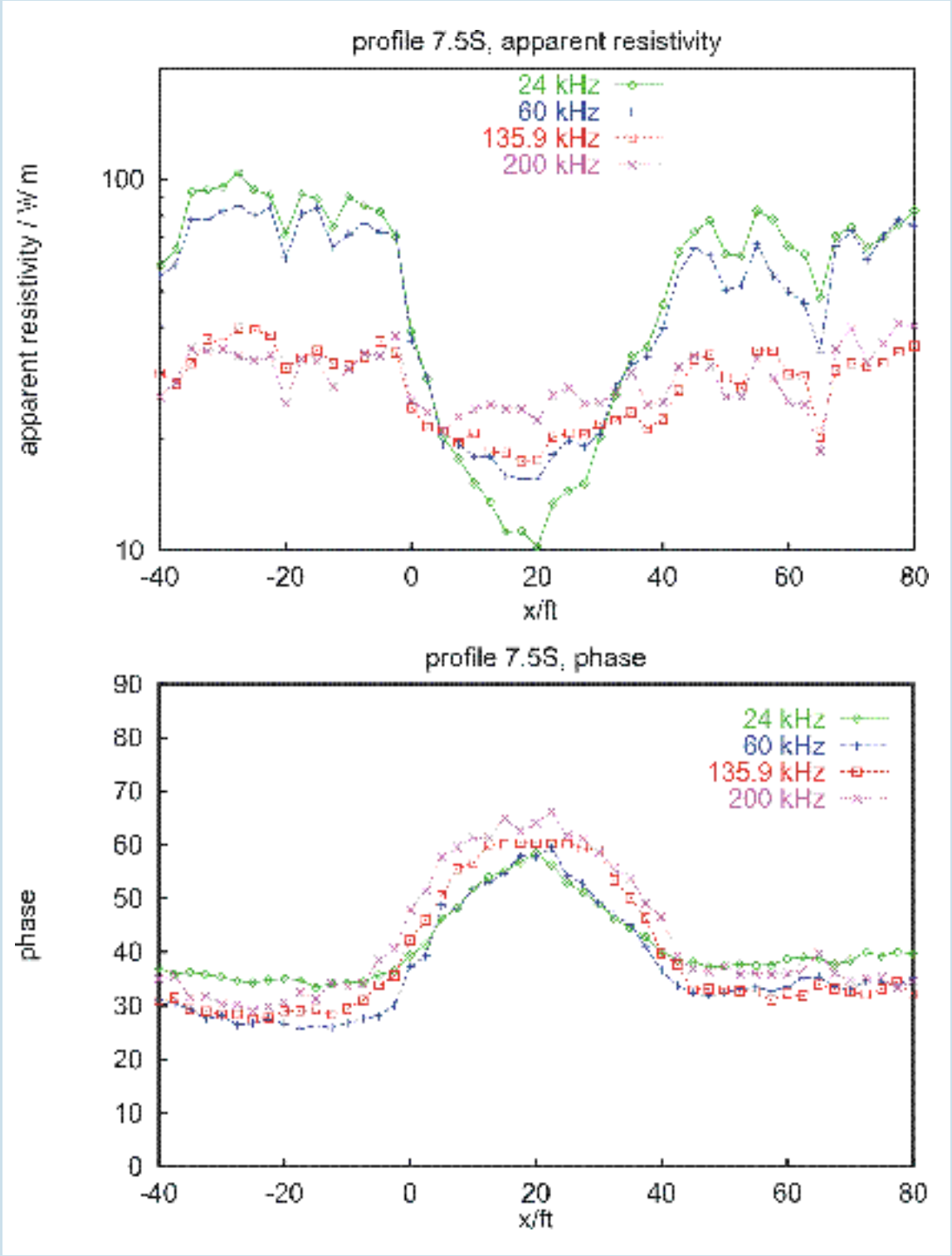

Fig. 39: Apparent resistivity and phase of profile 7.5S at the Idaho National Engineering Cold Test Pit. [5]

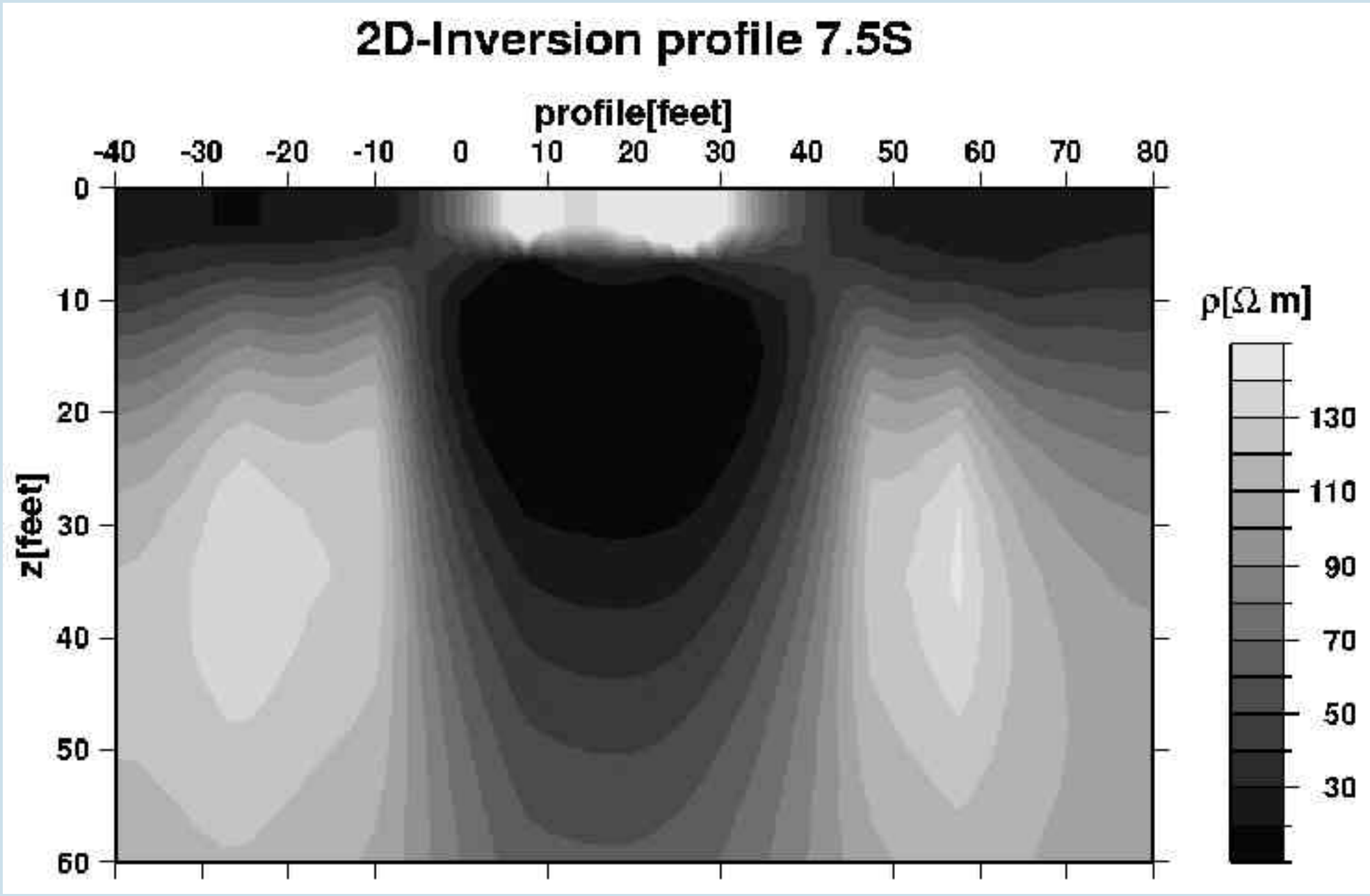

Fig. 40: A 2D conductivity model obtained from the RMT profile along 7.5S at the Idaho National Engineering Laboratory Cold Test Pit. [5]

3.7 Ground Penetrating Radar (GPR)

GPR is a technique of imaging the subsurface at high resolution.

Since the mid 1980s, GPR has become enormously popular, particular with the engineering and archaeological communities.

It was applied since the 1960s in connection with the development of radioechosounding of polar ice sheets. For regional and large-scale investigations, radar measurements have been made from aircraft and satellites.

➔ Ancient river drainage systems now buried beneath desert sands in Africa

➔ important source of possible water

In the GPR method, a short radar pulse in the frequency band 10MHz - 1GHz is introduced in the ground. The reflection of electromagnetic waves are observed.

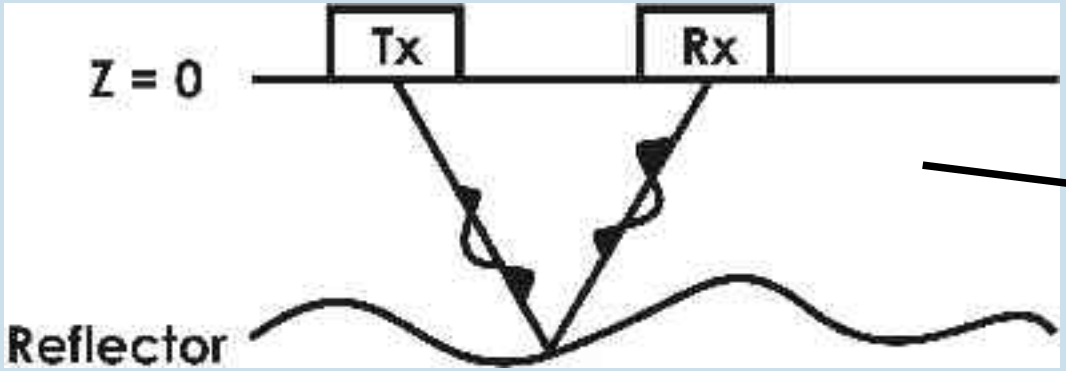

Fig. 41

$$v = \frac{c}{\sqrt{\epsilon_r \cdot \mu_r}}$$

Radar velocities are controlled by the dielectric constant ϵ_r where c is the velocity of light in vacuum ($3 \cdot 10^8$ m/s), and μ_r is the relative magnetic permeability which is close to unity for non-magnetic rocks.

A radar system comprises a signal generator, transmitting and receiving antennae and a receiver that may have recording facilities.

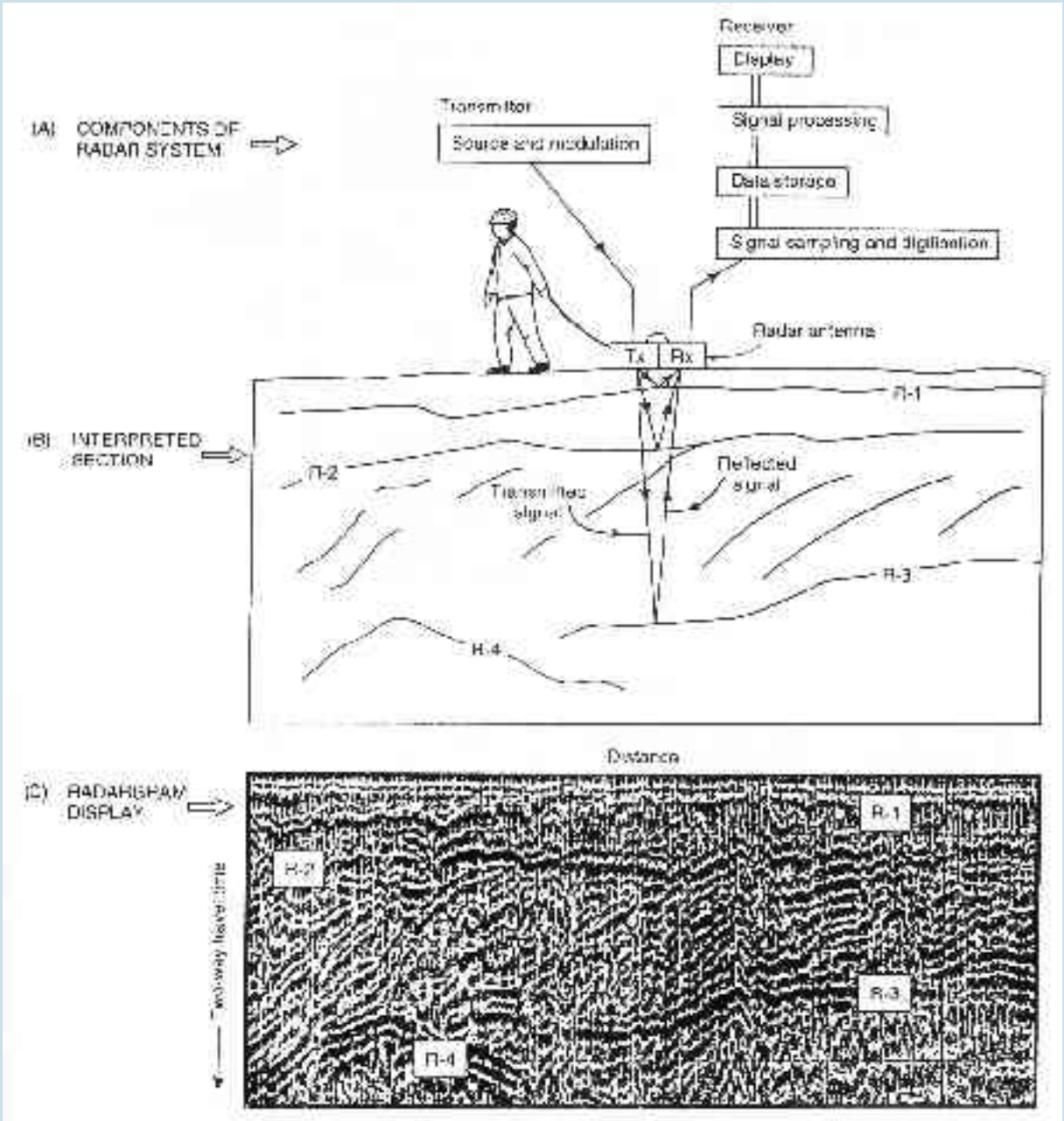

Fig. 42: Simplified diagram of (A) the constituents of a radar system with (B) the interpreted section of (C) the radargram display.[1]

Ground Penetrating Radar (GPR)

- As radiowaves travel at high speeds (in air 300 000 km/s), the travel time is a few tens to several thousand nanoseconds (ns=10^{-9}s). This requires a very accurate instrumentation to measure the signal.
- The antennae used can be in monostatic or bistatic mode.

monostatic: one antenna device is used as both transmitter and receiver

bistatic: two seperate anntennae are used with one serving as transmitter and the other as receiver

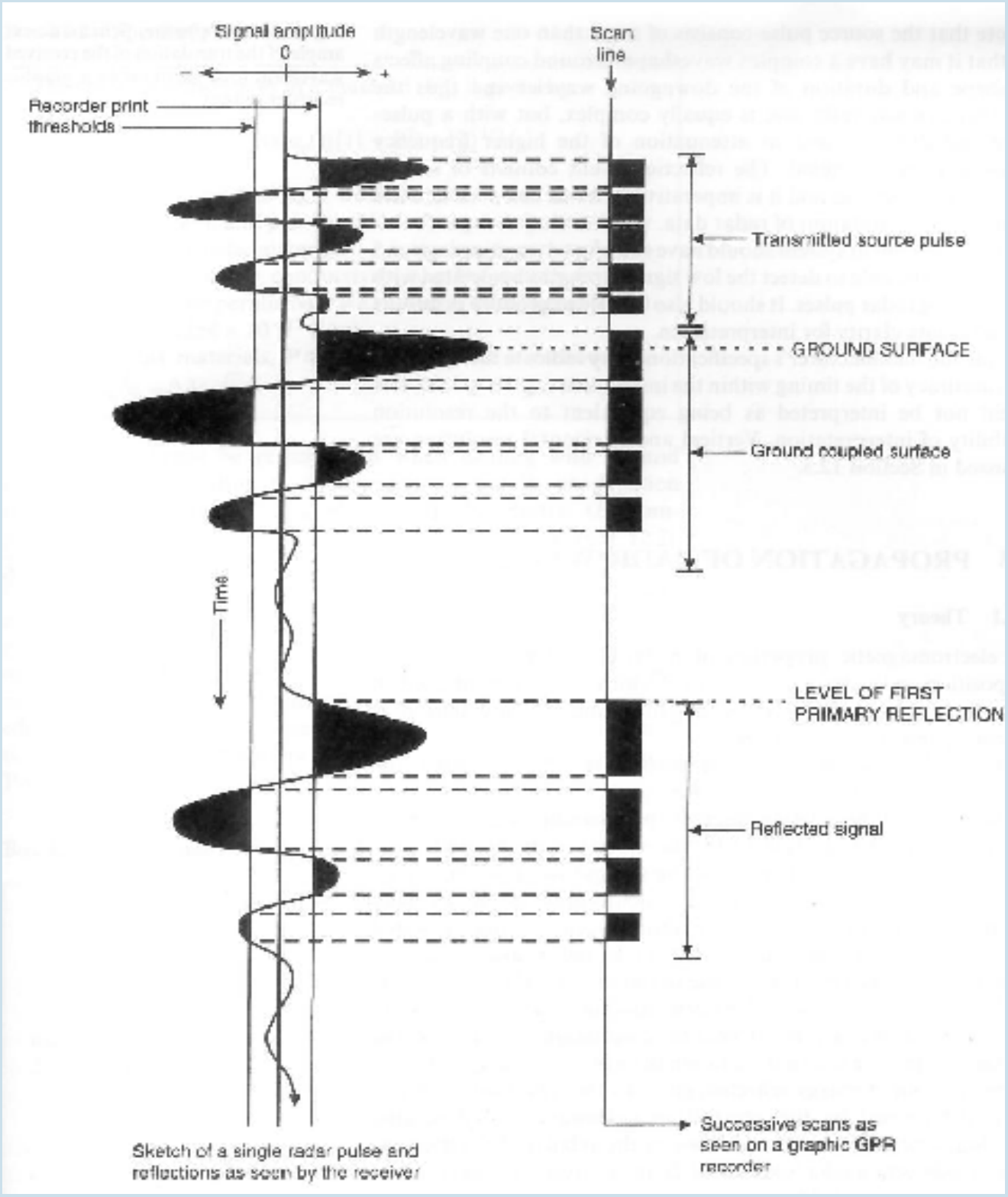

Fig. 43: Schematic example of the translation of the received waveform (one scan) on to a graphic recorder output.[1]

The depth of the reflector can be calculated from the travel time of the reflected signal:

$$d = \frac{t}{2} \cdot v$$

Ground Penetrating Radar (GPR)

A contrast in dielectric properties across an interface causes reflection of part of a radar pulse according to the reflection coefficient

$$R = \frac{\sqrt{\epsilon_{r_1}} - \sqrt{\epsilon_{r_2}}}{\sqrt{\epsilon_{r_1}} + \sqrt{\epsilon_{r_2}}} = \frac{v_2 - v_1}{v_2 + v_1}$$

where ϵ_{r_1} and ϵ_{r_2} are the relative permittivities (dielectric constants) of the two media seperated by the interface and v_1 and v_2 the radar velocities within them.

Velocities of geological materials lie within the range 0.06-0.175 m/ns.

Typical value for f=100MHz.

Ground Penetrating Radar (GPR)

material	ϵ_r	σ (ms/m)	v (m/ns)	α (dB/m)
water	80	0.5	33	0.1
dry sand	3 – 5	0.01	0.15	0.01 – 1
wet sand	20 – 30	0.1 – 1	0.06	0.03 – 0.3
clay	5 – 40	2 – 1000	0.06	1 – 300
granite	6	0.01 – 1	0.12	0.01 – 1

→ Water has a dielectric constant of 80.

The water content of materials exerts a strong influence on the propagation of a radar pulse.

Velocity contrast between dry and wet sand!

→ Groundwater exploration

Range of applications of GPR

- contaminant plume mapping
- landfill investigations
- location of buried fuel tanks and oil drums
- detection of natural cavities and fissures
- void detection
- ice thickness mapping
- location of buried archaeological objects

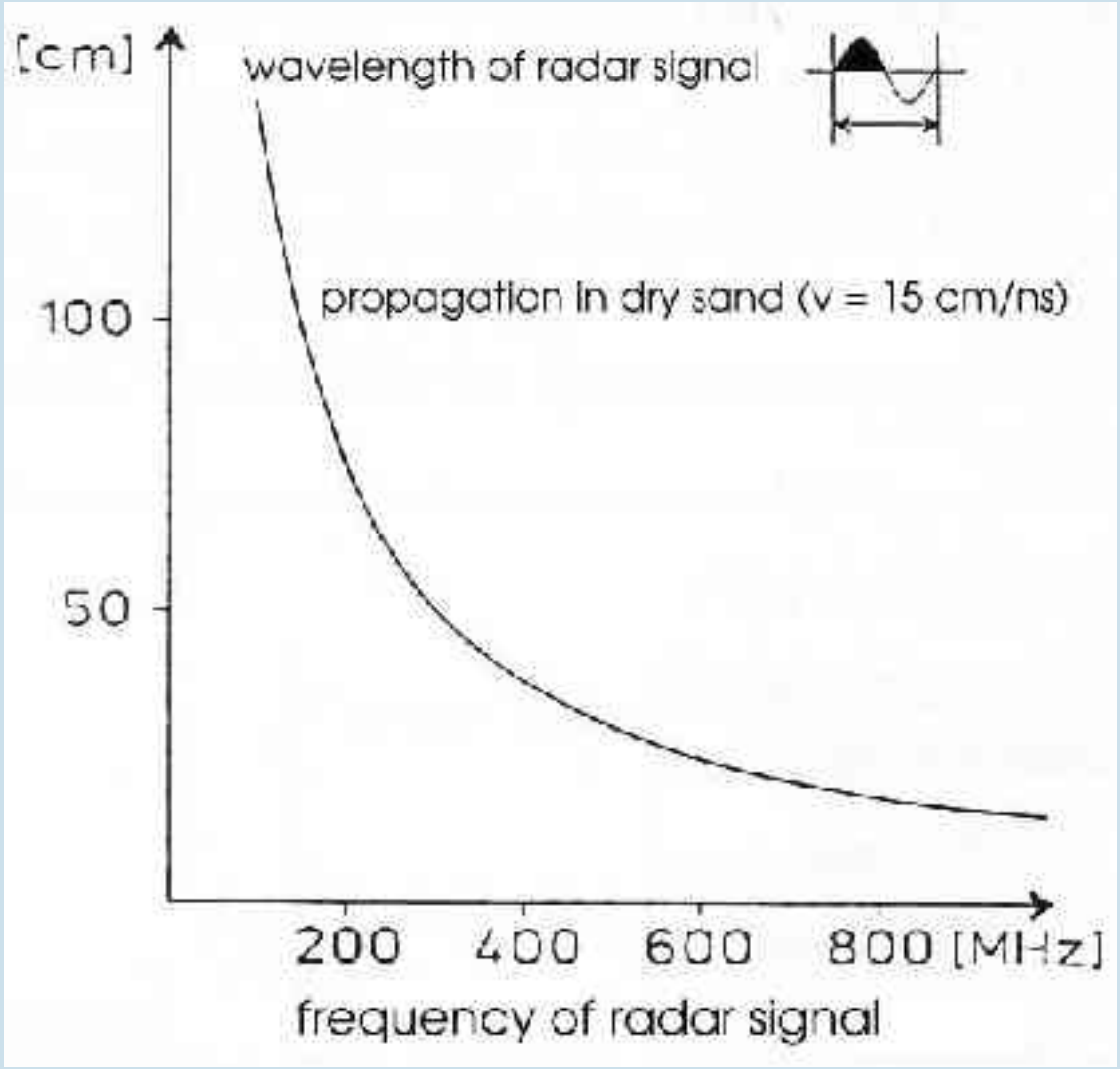

Fig. 44: Wavelength of electro-magnetic waves in dependence of signal frequency.[7]

Velocities of geological materials are very high
→ corresponding wavelengths are in the range of decimeter.
→ very good resolving of small structures

Attenuation

However, energy is lost due to attenuation α which is dependent upon the electric (σ), magnetic (μ) and dielectric (ϵ) properties of the geological medium as well as the frequency of the radar signal.

$$\frac{E_0}{E_x} = \exp(-\alpha x)$$

$$\alpha = \omega \left\{ \left(\frac{\mu \epsilon}{2} \right) \left[\left(1 + \frac{\sigma^2}{\omega^2 \epsilon^2} \right)^{1/2} - 1 \right] \right\}^{1/2}$$

→ small α values for air, ice, granite

→ ideal conditions for GPR

Penetration Depth

Penetration depth for georadar signal:

$$d[\mathrm{m}] = \frac{\rho[\Omega\,\mathrm{m}]}{30}$$

→ small penetration depths for rocks with low resistivities

clay: 0.8 - 1m
saturated sand ≈ 2m
dry sand ≈ 5m

3.7.1 Models of data acquisition

a) radar reflection profile:

The transmitter and receiver antennae are kept at a small, fixed seperation.

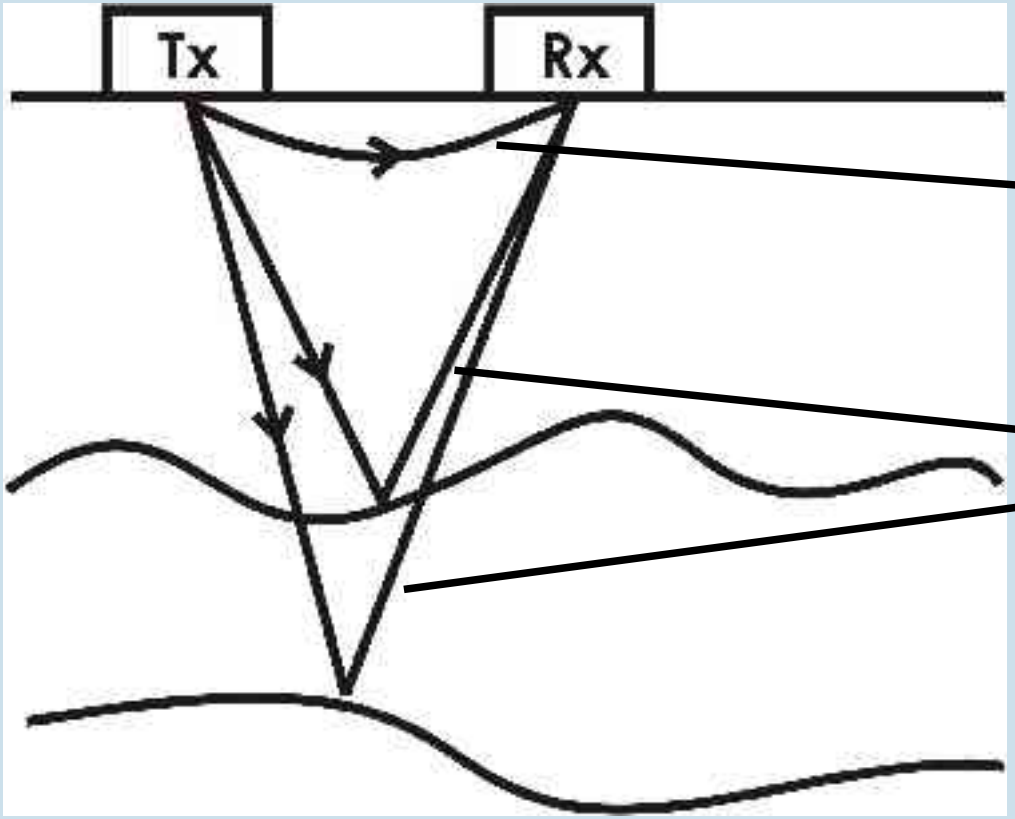

Fig. 45

Wave types

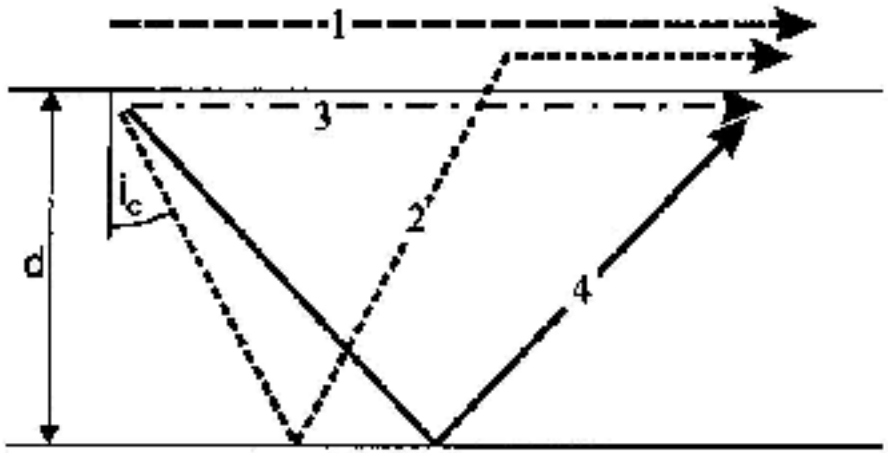

1. direct air wave
2. critically refracted air wave
3. direct ground wave
4. reflected wave sin $i_c = v_1/v_0$

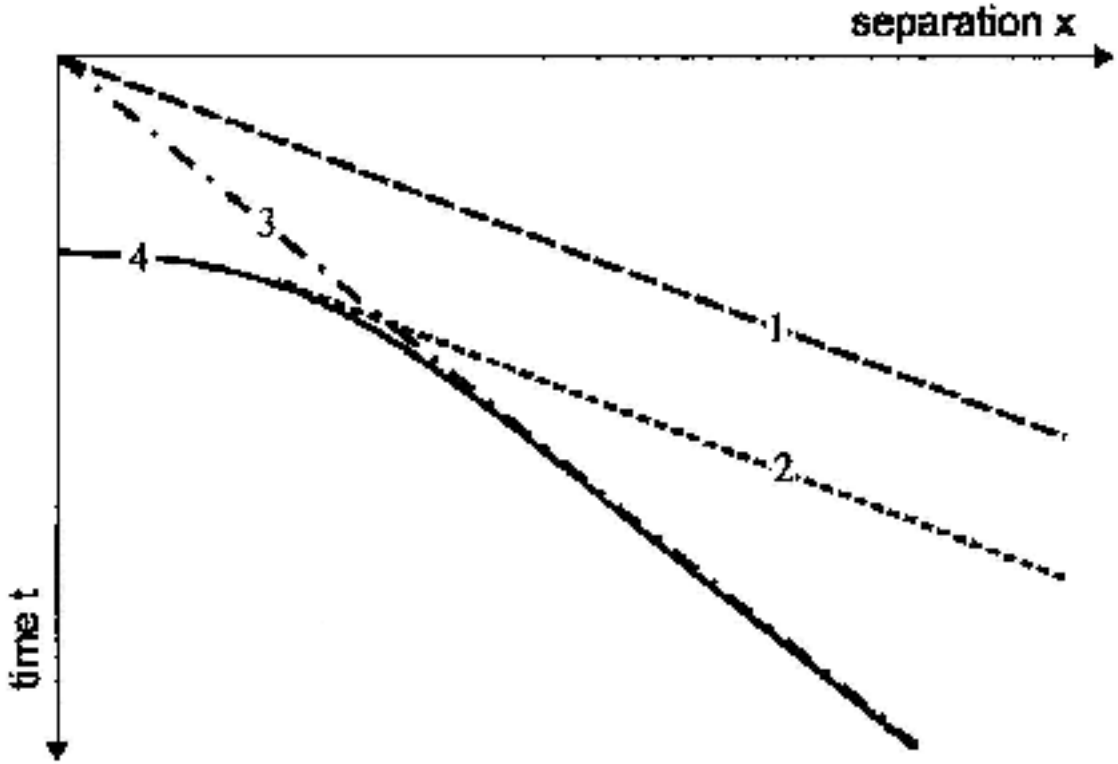

Fig. 46 [3]

Radargram

The observed signals can be summarized as radargram.

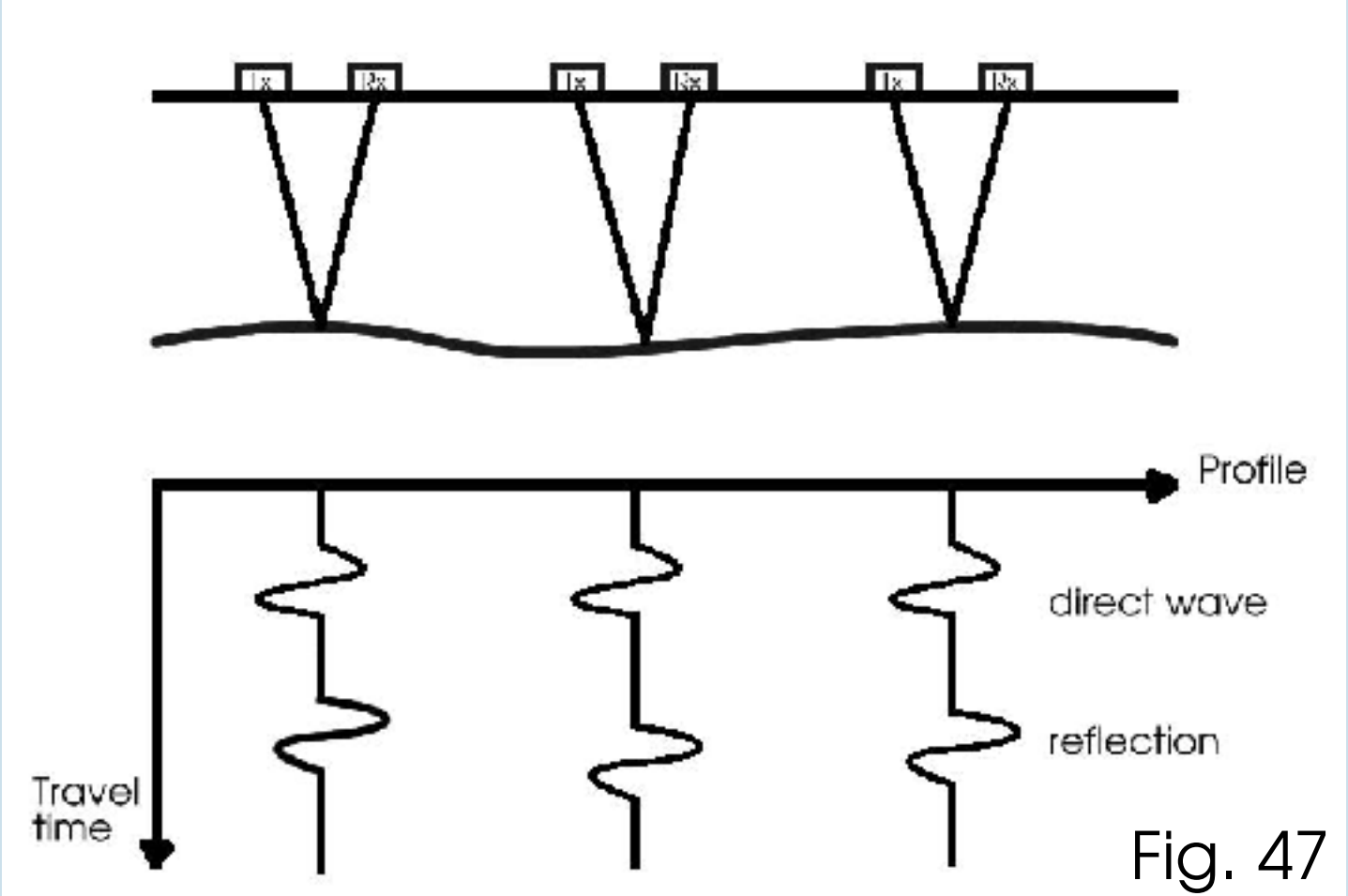

Fig. 47

Reflection

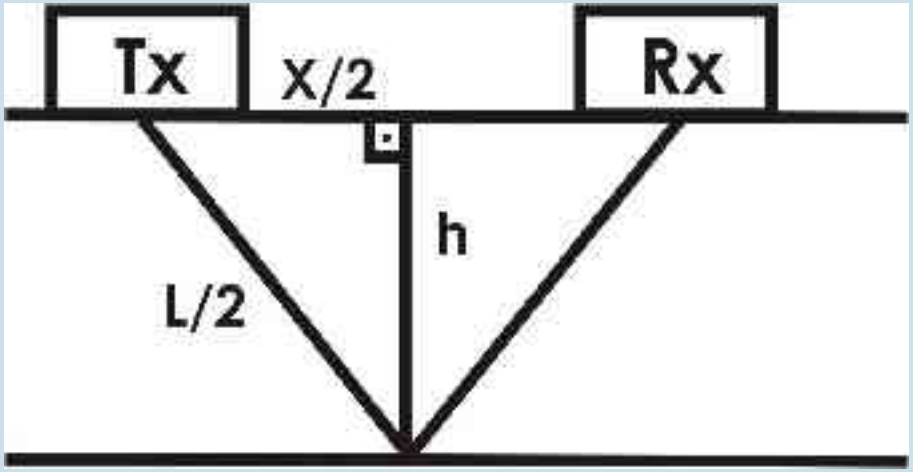

Fig. 48

$$(L/2)^2 = (x/2)^2 + h^2$$

$$\frac{L^2}{4} = \frac{x^2}{4} + h^2$$

$$L = \sqrt{x^2 + 4h^2}$$

$$\Rightarrow t = \frac{1}{v}\sqrt{x^2 + 4h^2}$$

Models of data acquisition

b) wide-angle reflection and refraction (WARR) sounding:
The transmitter is kept at a fixed location and the receiver is towed away at increasing offsets.

c) common-depth point (CDP) method:
Transmitter and receiver antennae are moved apart about a fixed central point.

b and c are designed to show how the radar velocities change with depth.

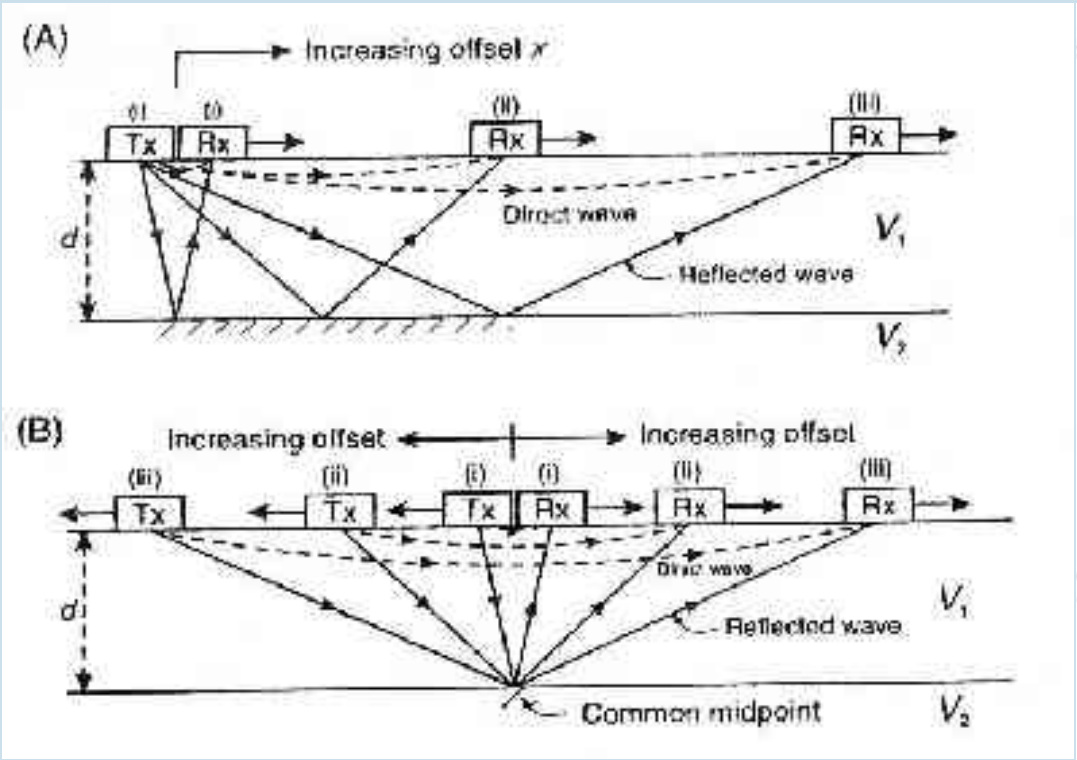

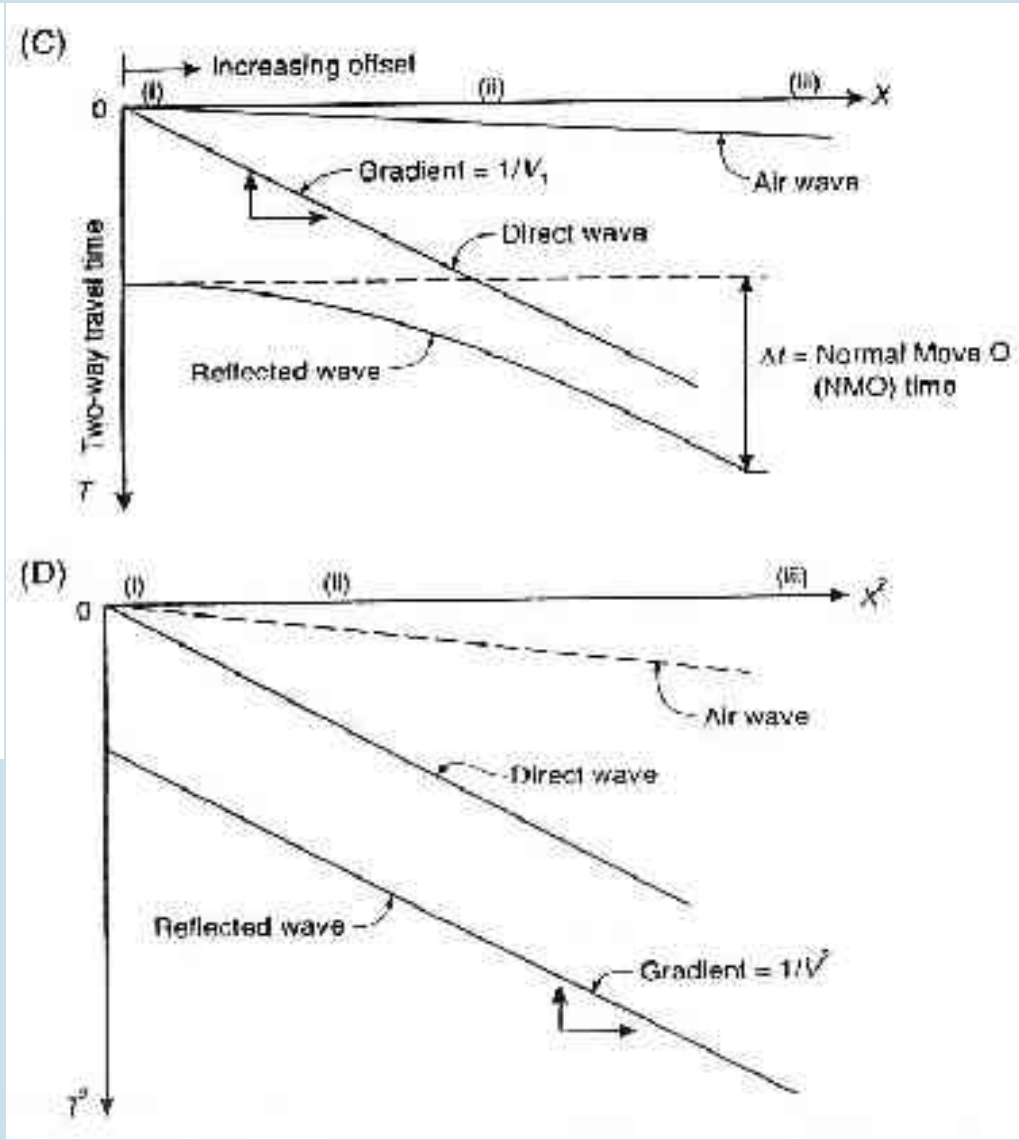

Fig. 49: (A) WARR sounding and (B) CMP sounding with (C) a time-distance moveout, and (D) the corresponding T^2-X^2 graph.[1]

Ground Penetrating Radar (GPR)

Resolving power

- vertical resolving: $\frac{\lambda}{4}$
- horizontal resolving: $\sqrt{\frac{z \cdot \lambda}{4}}$

where $\lambda = \frac{v}{f}$

Example: $f = 100\,\mathrm{MHz}, v = 0.1\,\mathrm{m/ns} \quad \Rightarrow \lambda = 3\,\mathrm{m}$

The structures in the radargram

- local small anomalies: buried tanks, pipes ⇒ hyperbola
- horizontal reflections: groundwater horizonts

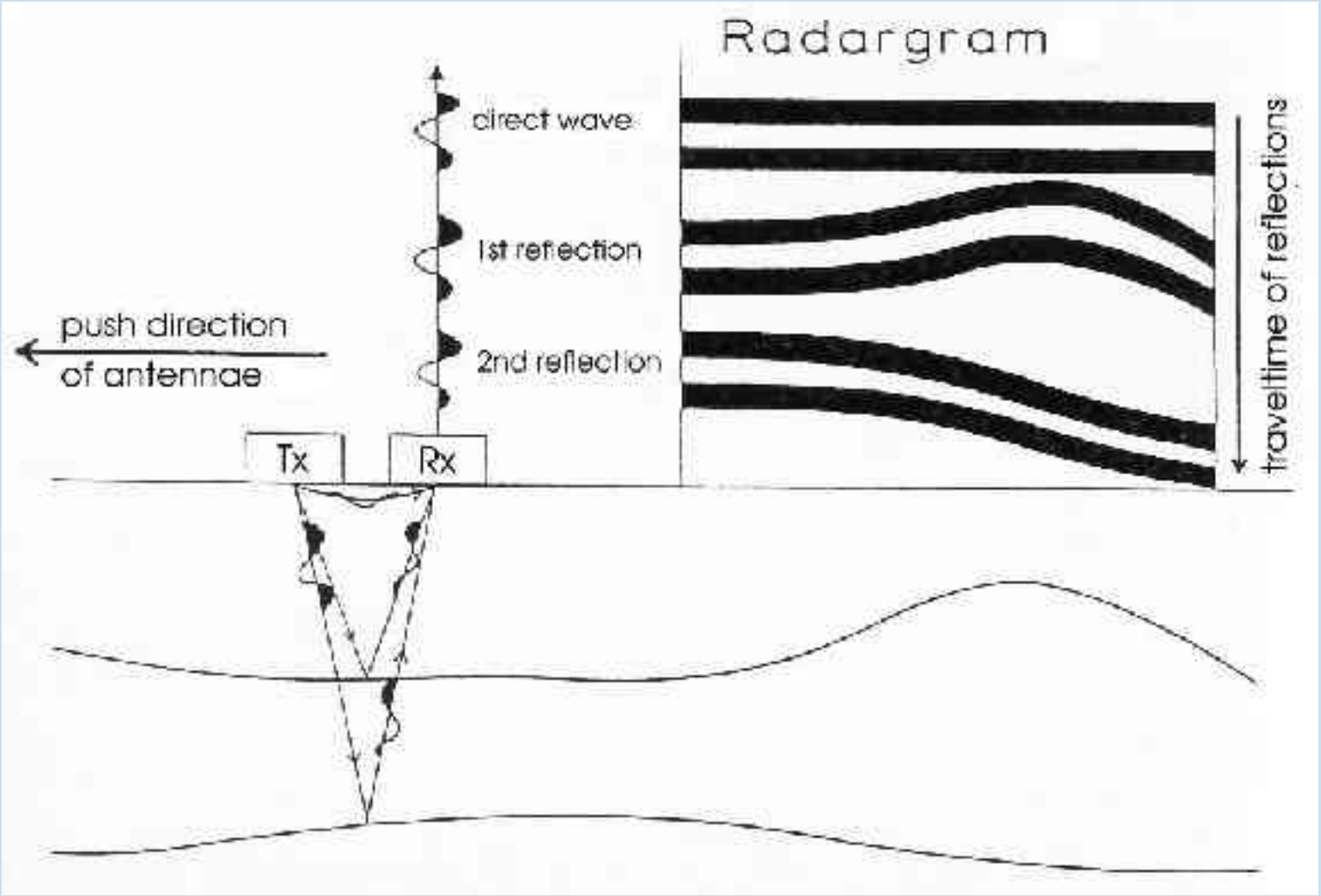

Fig. 50: Origin of a radargram.[7]

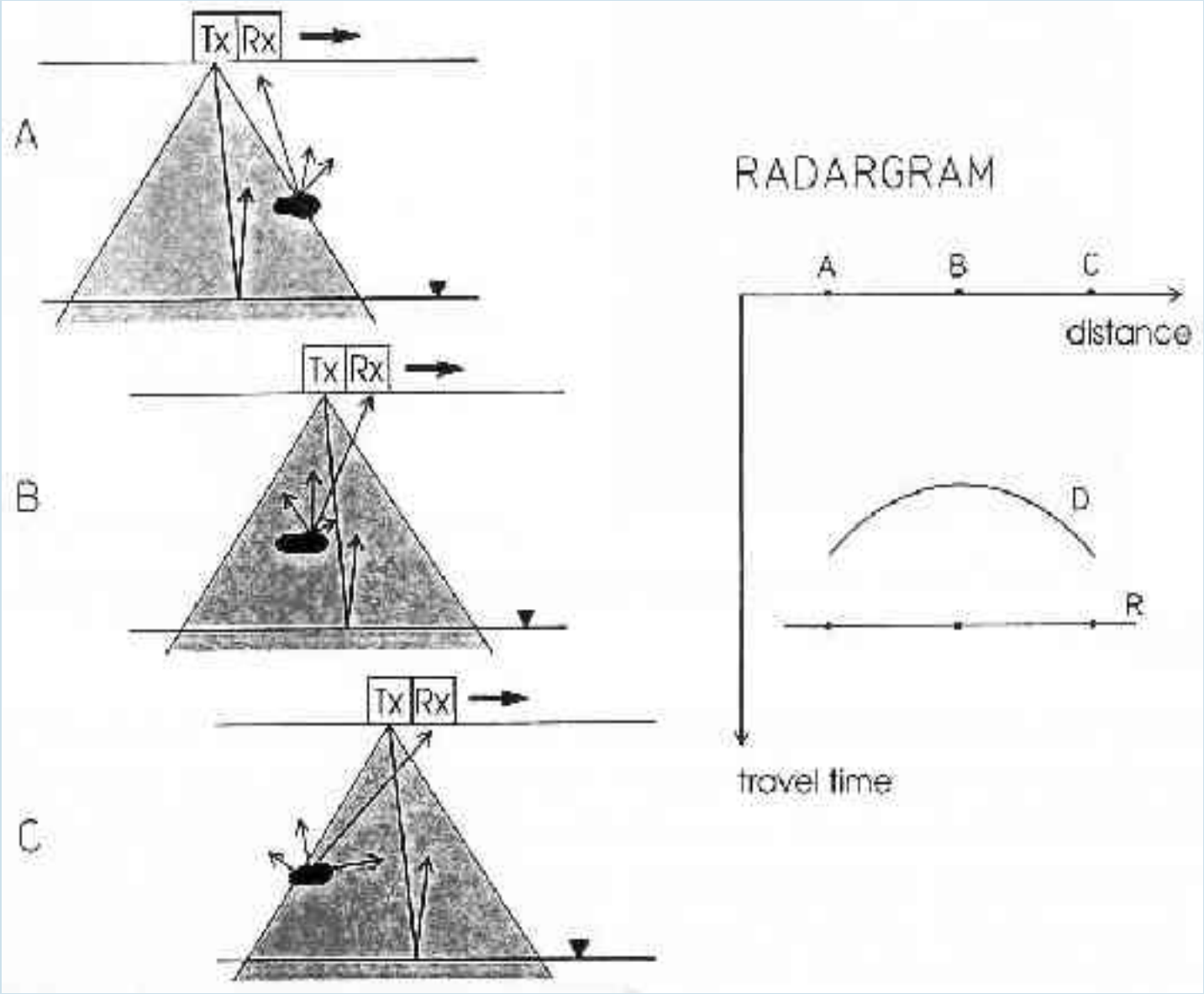

Fig. 51: Schematic graph of the origin of diffraction.
Tx: transmitter antenna, Rx: receiver antenna,
R: reflection of groundwater table, D: diffraction.[7]

3.7.2 Case Studies

Fig. 52: Measurements with Ground Penetrating Radar. Left: 120 MHz antenna system (bistatic). Right: 500 MHz antenna system (monostatic).[7]

Case Studies

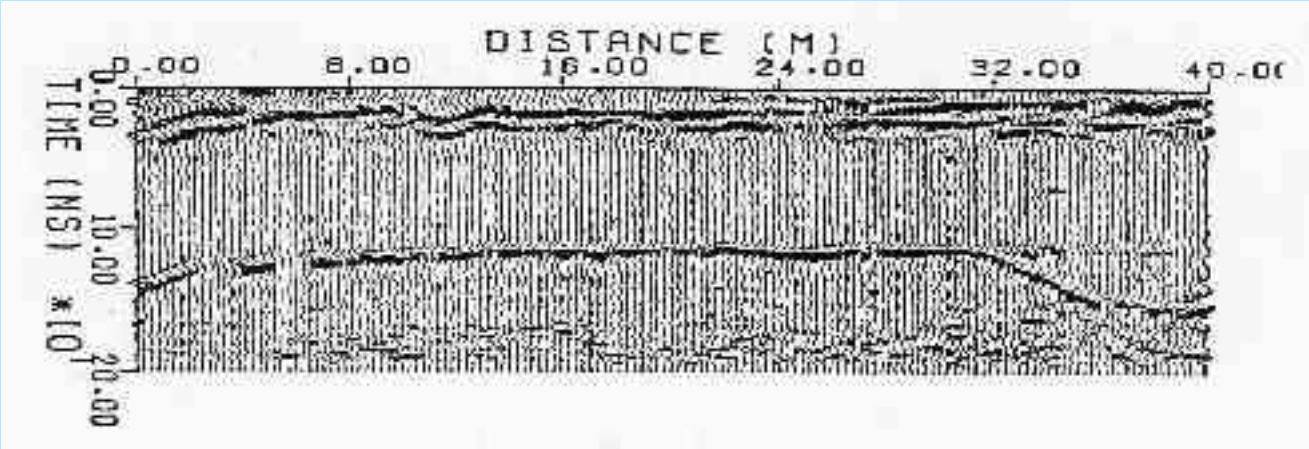

Fig. 53: Example of a radargram: The reflector at 12 ns is caused by a sand/clay boundary.

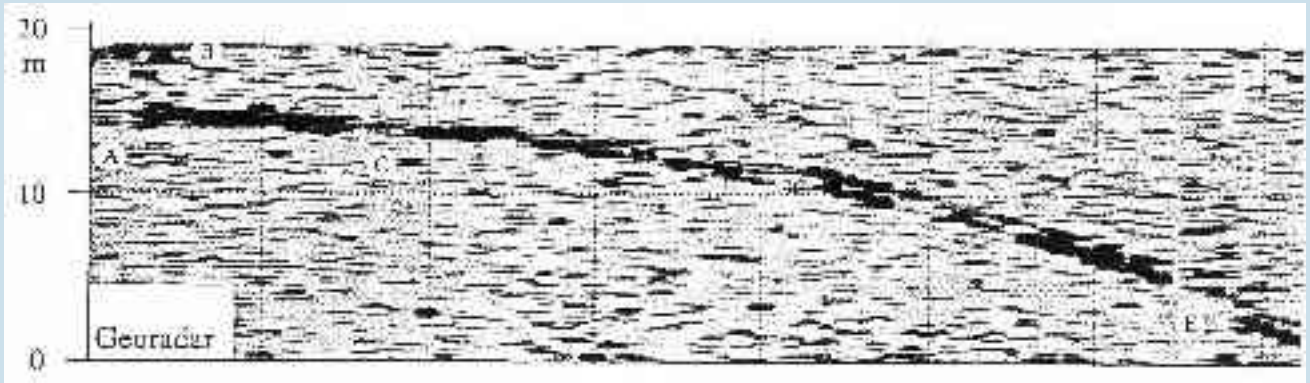

Fig. 54: Areal view of a radar mapping. The figure shows the outlines of an antique water pipe.[7]

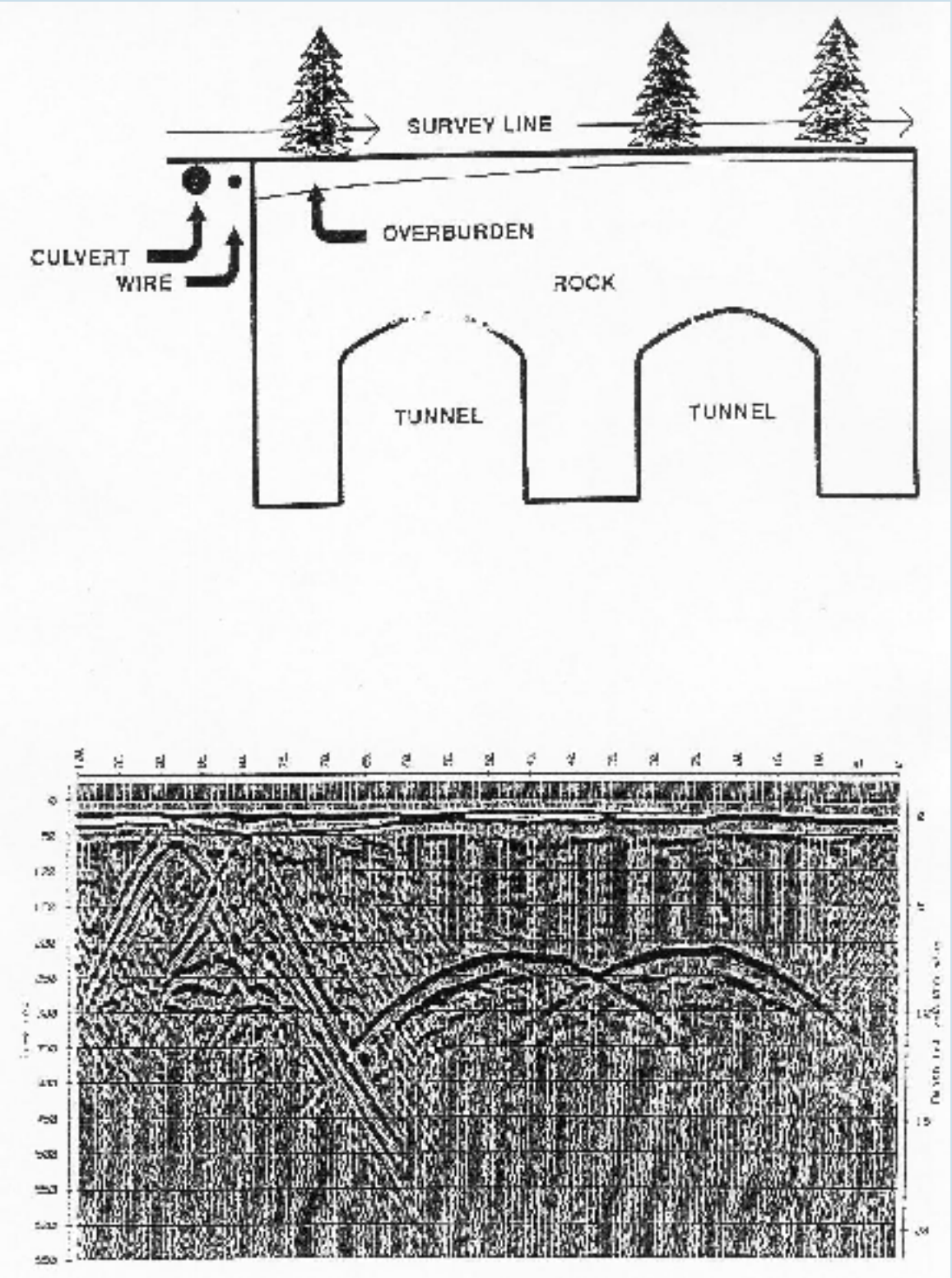

Fig. 55

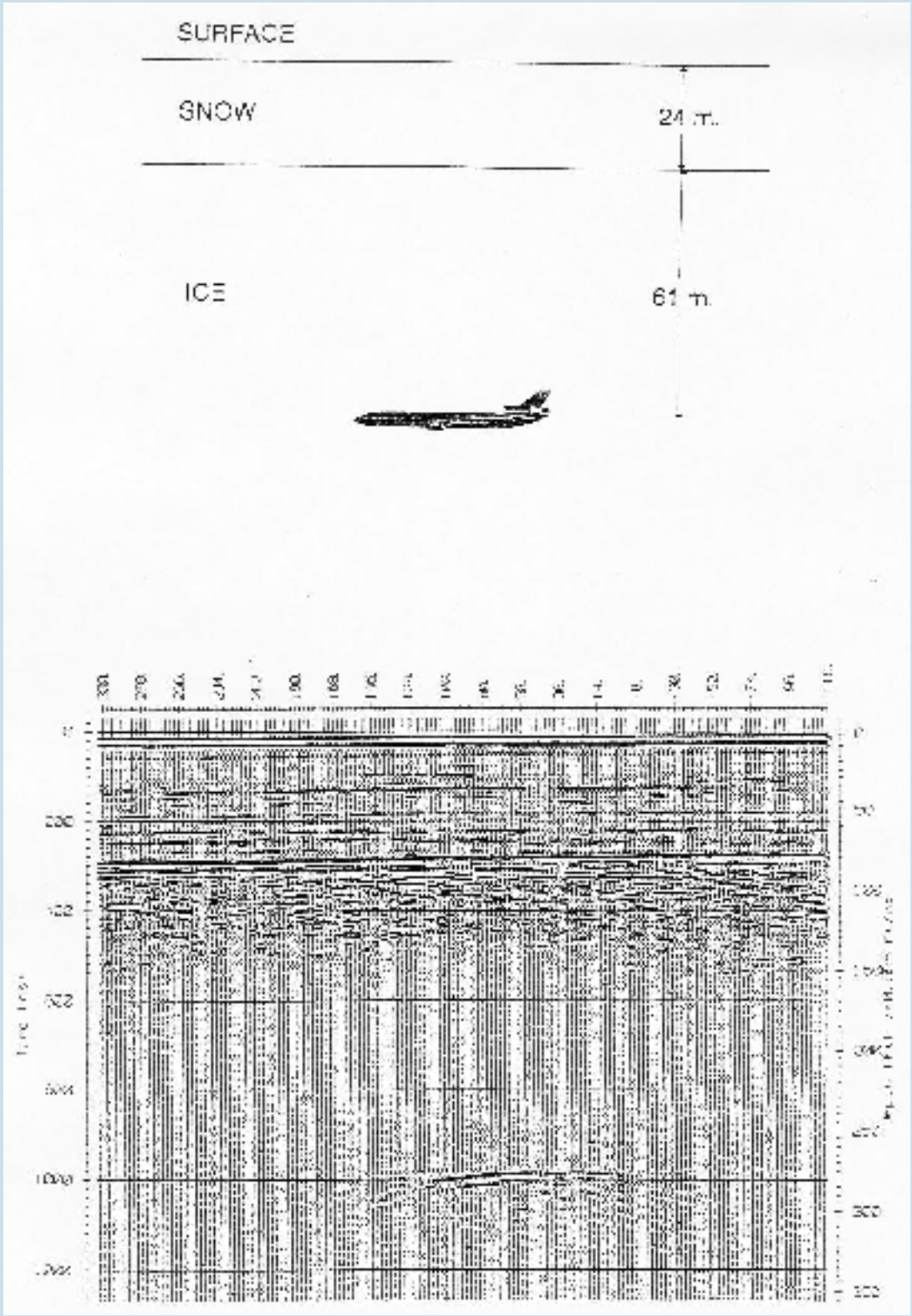

Fig. 56

References

1) Reynolds, J. M.: An Introduction to Applied and Environmental Geophysics, Wiley, 1998

2) Kearey, P., Brooks, M.: An Introduction to Geophysical Exploration, Blackwell, 2002

3) Dietrich, P.: Introduction to Applied Geophysics, Script, Sept. 2002

4) Vogelsang, D.: Environmental Geophysics, A Practical Guide, Springer Verlag, 1995

5) Tezkan, B.: A review of environmental applications of quasi-stationary electromagnetic techniques, Surveys in Geophysics, 1999, 20, 279-308

References

6) Wilsom, J.: Field Geophysics, Wiley,1989

7) Kirsch, R.: Umweltgeophysik in der Praxis: Untersuchung von Altablagerungen und kontaminierten Standorten, Script